



**NAVAL
POSTGRADUATE
SCHOOL**

MONTEREY, CALIFORNIA

THESIS

**A THREE-PHASE HYBRID DC-AC INVERTER SYSTEM
UTILIZING HYSTERESIS CONTROL**

by

Terence H. White

June 2004

Thesis Advisor:
Second Reader:

Robert Ashton
Xiaoping Yun

Approved for public release; distribution is unlimited

THIS PAGE INTENTIONALLY LEFT BLANK

REPORT DOCUMENTATION PAGE			Form Approved OMB No. 0704-0188	
Public reporting burden for this collection of information is estimated to average 1 hour per response, including the time for reviewing instruction, searching existing data sources, gathering and maintaining the data needed, and completing and reviewing the collection of information. Send comments regarding this burden estimate or any other aspect of this collection of information, including suggestions for reducing this burden, to Washington headquarters Services, Directorate for Information Operations and Reports, 1215 Jefferson Davis Highway, Suite 1204, Arlington, VA 22202-4302, and to the Office of Management and Budget, Paperwork Reduction Project (0704-0188) Washington DC 20503.				
1. AGENCY USE ONLY (Leave blank)		2. REPORT DATE June 2004	3. REPORT TYPE AND DATES COVERED Master's Thesis	
4. TITLE AND SUBTITLE: A Three-Phase Hybrid DC-AC Inverter System Utilizing Hysteresis Control			5. FUNDING NUMBERS	
6. AUTHOR(S) Terence White			8. PERFORMING ORGANIZATION REPORT NUMBER	
7. PERFORMING ORGANIZATION NAME(S) AND ADDRESS(ES) Naval Postgraduate School Monterey, CA 93943-5000			10. SPONSORING/MONITORING AGENCY REPORT NUMBER	
9. SPONSORING /MONITORING AGENCY NAME(S) AND ADDRESS(ES) N/A			11. SUPPLEMENTARY NOTES The views expressed in this thesis are those of the author and do not reflect the official policy or position of the Department of Defense or the U.S. Government.	
12a. DISTRIBUTION / AVAILABILITY STATEMENT Approved for public release, distribution is unlimited			12b. DISTRIBUTION CODE	
13. ABSTRACT (maximum 200 words) The naval vessels of the future will require lighter, more compact, and more versatile power electronics systems. With the advent of the DC Zonal Electrical Distribution System, more innovative approaches to the conversion of the dc bus power to ac power for motor drives will enhance the efficiency and warfighting capability of tomorrow's ships. This thesis explores the concept of a hybrid dc-ac power converter that combines a hysteresis controlled inverter with a six-step bulk inverter. A six-step bulk inverter is built from discrete components and tested in simulation and hardware. The two inverters are connected in parallel to provide a high-fidelity current source for a three-phase load. The addition of the hysteresis inverter to the bulk inverter adds a closed current loop for more robust control and improves the quality of the output load current.				
14. SUBJECT TERMS Hybrid inverter, hysteresis control, inverter, parallel inverters, six-step inverter, shipboard motor drives.			15. NUMBER OF PAGES 93	
			16. PRICE CODE	
17. SECURITY CLASSIFICATION OF REPORT Unclassified	18. SECURITY CLASSIFICATION OF THIS PAGE Unclassified	19. SECURITY CLASSIFICATION OF ABSTRACT Unclassified	20. LIMITATION OF ABSTRACT UL	

NSN 7540-01-280-5500

Standard Form 298 (Rev. 2-89)
Prescribed by ANSI Std. Z39-18

THIS PAGE INTENTIONALLY LEFT BLANK

Approved for public release; distribution is unlimited

**A THREE-PHASE HYBRID DC-AC INVERTER SYSTEM UTILIZING
HYSTERESIS CONTROL**

Terence H. White
Major, United States Marine Corps
B.S., University of California, Los Angeles, 1991

Submitted in partial fulfillment of the
requirements for the degree of

**MASTER OF SCIENCE IN
ELECTRICAL ENGINEERING**

from the

**NAVAL POSTGRADUATE SCHOOL
June 2004**

Author: Terence H. White

Approved by: Robert W. Ashton
Thesis Advisor

Xiaoping Yun
Second Reader

John P. Powers
Chairman, Department of Electrical and Computer
Engineering

THIS PAGE INTENTIONALLY LEFT BLANK

ABSTRACT

The naval vessels of the future will require lighter, more compact, and more versatile power electronics systems. With the advent of the DC Zonal Electrical Distribution System, more innovative approaches to the conversion of the dc bus power to ac power for motor drives will enhance the efficiency and warfighting capability of tomorrow's ships. This thesis explored the concept of a hybrid dc-ac power converter that combines a hysteresis controlled inverter with a six-step bulk inverter. A six-step bulk inverter was built from discrete components and tested in simulation and hardware. The two inverters were connected in parallel to provide a high-fidelity current source for a three-phase load. The addition of the hysteresis inverter to the bulk inverter added a closed current loop for more robust control and improved the quality of the output load current.

THIS PAGE INTENTIONALLY LEFT BLANK

TABLE OF CONTENTS

I.	INTRODUCTION.....	1
A.	RESEARCH GOALS.....	2
B.	SCOPE OF THESIS	2
II.	BACKGROUND INFORMATION	5
A.	INVERTER BASICS.....	5
B.	HYSTERESIS CONTROL	10
C.	HYBRID INVERTERS	12
III.	SYSTEM DESIGN AND DEVELOPMENT	17
A.	OVERALL SYSTEM DESIGN	17
B.	HYSTERESIS INVERTER.....	18
C.	BULK INVERTER.....	21
D.	SYSTEM CONFIGURATION	27
IV.	THEORETICAL RESULTS	29
A.	OVERALL PERFORMANCE	29
B.	HYSTERESIS INVERTER CURRENT	30
C.	BULK INVERTER CURRENT	31
V.	EXPERIMENTAL RESULTS	41
A.	PRELIMINARY TESTING OF BULK INVERTER	41
B.	THREE-PHASE TESTING OF HYSTERESIS INVERTER	43
C.	SINGLE-PHASE PARALLEL TESTING.....	44
D.	THREE-PHASE PARALLEL TESTING.....	45
E.	ZERO-SEQUENCE CURRENT	52
F.	SUMMARY OF RESULTS	54
VI.	CONCLUSION.....	57
A.	REVIEW OF RESEARCH QUESTIONS AND GOALS.....	57
B.	SUMMARY OF EXPERIMENTAL RESULTS.....	57
C.	ANSWERS TO RESEARCH QUESTIONS BASED ON RESULTS... 58	
D.	RECOMMENDATIONS FOR FURTHER DEVELOPMENT	58
APPENDIX A.	CIRCUIT WIRING DIAGRAMS	61
APPENDIX B.	MATLAB SIMULATION CODE	69
	LIST OF REFERENCES.....	73
	INITIAL DISTRIBUTION LIST	75

THIS PAGE INTENTIONALLY LEFT BLANK

LIST OF FIGURES

Figure 1.	Half-Bridge Inverter Circuit Topology.....	5
Figure 2.	Pulse-width modulation reference and carrier signals	8
Figure 3.	Typical Sine-PWM applied load voltage (From Reference 3).	9
Figure 4.	Hysteresis band for inverter control.....	11
Figure 5.	Topology of series-connected hybrid inverter (from Reference 2).	13
Figure 6.	Hybrid current-source/voltage source inverter (From Reference 5). ...	14
Figure 7.	Overall system block diagram of hybrid inverter system.	18
Figure 8.	Controller section of hysteresis inverter (From Reference 2).	19
Figure 9.	Power section of hysteresis inverter (From Reference 2).	20
Figure 10.	Block diagram of hysteresis inverter (After Reference 2).	20
Figure 11.	System block diagram of bulk inverter controller.	21
Figure 12.	60-Hz signal generator circuit (After Reference 6).	22
Figure 13.	Phase-shifter circuit (After Reference 7).	22
Figure 14.	Comparator circuit to generate logic signals to switches.	23
Figure 15.	Hysteresis signal reference circuit.....	24
Figure 16.	Amplifier circuit for square wave signal.	26
Figure 17.	Gate Driver Circuit (After Reference 8).	26
Figure 18.	Power section topology of hybrid inverter.	28
Figure 19.	Topology of single phase of hybrid inverter.	29
Figure 20.	Phase A applied voltage for bulk inverter (From Reference 3).	31
Figure 21.	Results of simulation of bulk inverter, phase A.	34
Figure 22.	Phase A, B, and C currents of the bulk inverter ($DV_{dc} = 39 \text{ V}$)	36
Figure 23.	Theoretical harmonic content of bulk inverter phase current.	38
Figure 24.	Bulk inverter phase current and voltage.	42
Figure 25.	Phases A (top), B (middle), and C (bottom) of hysteresis inverter operating independently with $I_h = 0.1 \text{ A}$ and $DV_{dc} = 39 \text{ V}$. (5.0 A/div). 44	
Figure 26.	Phases A, B, and C in parallel operation (5.0 A/div).	46
Figure 27.	Detailed view of phase A, B, and C currents (2.5 A/div).	47
Figure 28.	Frequency spectrum of bulk inverter (10 dB/div, 0-2000 Hz).	48
Figure 29.	Frequency spectrum of hybrid inverter (10 dBV/div, 0-2000 Hz).	49
Figure 30.	Hybrid Phase A – Bulk and Hysteresis phase currents (2A/div).	50
Figure 31.	Hybrid Phase B – Bulk and Hysteresis phase currents (2 A/div).	51
Figure 32.	Hybrid Phase C – Bulk and Hysteresis phase currents (2 A/div).	52
Figure 33.	Effect of zero-sequence current on hybrid circuit (2 A/div)	53
Figure 34.	Component Layout Diagram for Bulk Inverter Controller.....	61
Figure 35.	Component Layout Diagram for Hysteresis Signal Reference Circuit.	65

THIS PAGE INTENTIONALLY LEFT BLANK

LIST OF TABLES

Table 1.	Switching algorithm for six-step bulk inverter	32
Table 2.	Socket A wiring diagram	61
Table 3.	Socket B wiring diagram	62
Table 4.	Socket C wiring diagram	62
Table 5.	Socket D wiring diagram	62
Table 6.	Socket E wiring diagram	63
Table 7.	Socket F wiring diagram.....	63
Table 8.	Socket G wiring diagram	63
Table 9.	Socket H wiring diagram	63
Table 10.	Socket I wiring diagram	64
Table 11.	Socket J wiring diagram	64
Table 12.	Socket K wiring diagram	64
Table 13.	Socket L wiring diagram	64
Table 14.	Socket M wiring diagram	65
Table 15.	Socket N wiring diagram	66
Table 16.	Socket P wiring diagram	66
Table 17.	Socket Q wiring diagram	66
Table 18.	Socket S wiring diagram	67
Table 19.	Socket T wiring diagram.....	67
Table 20.	Potentiometer (R_i) connections	67

THIS PAGE INTENTIONALLY LEFT BLANK

ACKNOWLEDGMENTS

I would like to take the opportunity to recognize the people who helped me along the way in my research.

Thanks to all of the faculty and staff of the Naval Postgraduate School for your expertise and dedication. It was a privilege to study at your fine institution.

I would also like to thank all of my fellow officer students who always inspired me with their professionalism and kept me motivated through two years of study.

Most of all, thank you to my wife, Kathy, and my daughters, Natalie and Chloe, for all of your love and support.

THIS PAGE INTENTIONALLY LEFT BLANK

EXECUTIVE SUMMARY

This thesis continues an ongoing research effort to explore the concept of hysteresis control to produce a high-fidelity current source inverter for use in shipboard motor drives. The hybrid inverter system developed in this thesis addresses the fleet requirement for lighter and more compact power converters in the proposed advanced electrical power system for future naval vessels.

A six-step bulk inverter was designed, built, and tested prior to coupling with an existing hysteresis-controlled inverter. The two inverter elements were connected in parallel across a three-phase wye-connected load to form a hybrid inverter system. The hybrid inverter system capitalized on the high power capability of the bulk inverter and the closed-loop current control employed by the hysteresis inverter. The goal of the research was to demonstrate that the parallel combination of the six-step bulk inverter and the hysteresis inverter could produce a high-fidelity load current. Experimental trials attempted to optimize the system configuration to draw all of the current at the fundamental frequency from the six-step bulk inverter and utilize the hysteresis inverter to improve the quality of the current waveform.

The experimental testing showed that both the bulk inverter and the hysteresis inverter operated as designed when connected to an inductive three-phase load with a floating neutral point. The two inverters operated well when connected in parallel across a three-phase load. When the hysteresis inverter was added to the bulk inverter, the total harmonic distortion of the phase current waveform dropped from 5.5% to 3.2%. The overall current waveforms for all three phases closely corresponded to the reference current signal and the hybrid inverter produced a stable, sinusoidal load current. The magnitude of the phase current was set at 5.0 A peak across a load consisting of an inductance of 9.1 mH and a resistance of 1.05 Ω .

The primary input variables were the dc bus voltage, phase shift between the bulk and hysteresis inverter reference signals, and width of the hysteresis band. These input variables were adjusted to optimize the hybrid inverter system in order force the bulk inverter to produce as much of the fundamental load current as possible. The optimal experimental results were found with the dc bus voltage set at 30.8 V, the phase shift at 55° , and the width of the hysteresis band at 0.1 A. Although the bulk inverter did supply most of the fundamental load current, the hysteresis inverter was still required to produce some of the fundamental. Theoretically with further controller refinement, the hysteresis inverter should only be needed to cancel the harmonic content of the bulk inverter.

The concept of a hybrid inverter consisting of a six-step bulk inverter and a hysteresis controlled inverter was validated in this experiment. Follow-on research including controller refinement and higher power testing can further develop the hybrid inverter for potential use on shipboard motor drives.

I. INTRODUCTION

As naval technology continues to advance, the power electronic systems installed in ships must become more efficient, versatile, and dependable. Innovation in methods to supply power to shipboard warfighting systems will provide the key to creating a modern and capable fleet. Electric motors perform a multitude of critical functions aboard all types of ships in the United States Navy, and they all need a clean and reliable source of power.

The proposed advanced electrical power system for future naval vessels features the DC Zonal Electric Distribution System (DC ZEDS) to provide a more efficient means of distributing power throughout the ships. This system will rely heavily on dc-ac inverters that are lighter and more compact than the systems that are available on the commercial market today. The Office of Naval Research (ONR) contends that the current conventional power electronics systems are too large and heavy, and mandates the development of unique power conversion solutions to implement in future naval power distribution systems [1]. One possible solution to improve the compactness and power quality of commercial products is presented in this thesis.

The hybrid inverter system represents a unique approach to the conversion of dc power to a three-phase ac supply capable of driving the various motors aboard today's naval vessels. The system would most likely consist of a large commercial bulk inverter paralleled or cascaded with a high bandwidth filtering inverter. With a simple, compact controller, the hybrid inverter developed in this thesis can provide a high-fidelity current source that can be scaled to match an array of applications. Utilizing the concept of hysteresis control, it can maintain a constant current to the load despite disturbances in the dc-link voltage. With two inverter elements connected in parallel, the hybrid inverter also provides a degree of redundancy for the power source to the motor.

A. RESEARCH GOALS

This thesis continues previous work began in Reference 2 to develop the concept of a hysteresis controlled inverter coupled in parallel with a six-step bulk inverter to produce a three-phase ac source for a motor drive. In the previous research effort, the hysteresis inverter was designed, built and tested as an independent unit. Preliminary testing was also done to verify that a single phase of the hysteresis inverter could work in parallel with a square-wave inverter.

The goals of the research effort are listed below.

- Design, build, and test a six-step bulk inverter capable of parallel operation with the hysteresis inverter.
- Operate the new six-step inverter in parallel with the existing three-phase hysteresis inverter across a wye-connected load.
- Determine if the hybrid combination of the hysteresis inverter and the bulk inverter can produce a high-fidelity output current.
- Test the hybrid inverter under various conditions to find the optimal operating point; produce all current at the fundamental frequency with the bulk inverter while the hysteresis inverter cancels higher order harmonics.

It is hoped that successful testing of the hybrid inverter would validate the hybrid system concept and mandate continued efforts to develop the system for shipboard use.

B. SCOPE OF THESIS

The design and construction of the six-step bulk inverter began the process of developing a hybrid inverter system. After testing the new bulk inverter to verify its capabilities, the existing hysteresis inverter was retested to assess its performance before paralleling. With two operable inverter elements, the hybrid inverter system was assembled and tested. After adjusting the bulk inverter so that it was producing all of the fundamental current, the hybrid inverter was stud-

ied in detail to determine the optimal operating point and measure its performance against research goals. This thesis details the research process and consists of the following chapters:

Chapter I introduces the topic and motivates the need for a novel dc-ac power conversion system.

Chapter II builds the reader's knowledge base on inverter theory and reviews some of the current literature on the topic of hybrid inverters.

Chapter III describes the process of the design and development of the components of the hybrid inverter system. The overall system level diagrams and the details of each circuit appear here.

Chapter IV discusses the governing theory that will predict the performance of each inverter element. The predicted performance of the bulk inverter is projected with a computer simulation.

Chapter V presents the results of each phase of the experimental testing. The results are weighed against the predicted performance and research goals.

Chapter VI summarizes the complete results of this thesis and provides recommendations for future research work geared to further develop the hybrid inverter concept. Wiring diagrams, layout diagrams, MATLAB computer simulation code, and relevant component data sheets can be found in the Appendices.

THIS PAGE INTENTIONALLY LEFT BLANK

II. BACKGROUND INFORMATION

This chapter familiarizes the reader with the technical concepts covered in the thesis. The basics of inverters and the various inverter control strategies are introduced. The chapter also includes a review of current research on hybrid inverters.

A. INVERTER BASICS

As a critical component of most large motor drive systems, an inverter converts a dc power source into a controlled sinusoidal input current for the motor at a desired operating frequency; the dc power is generally derived by rectifying an ac generating source. The inverter uses a network of switches to alternate the positive and negative voltage buses of the input dc source to produce the ac voltage across the load [3]. A representation of a simple half-bridge inverter circuit is depicted in Figure 1.

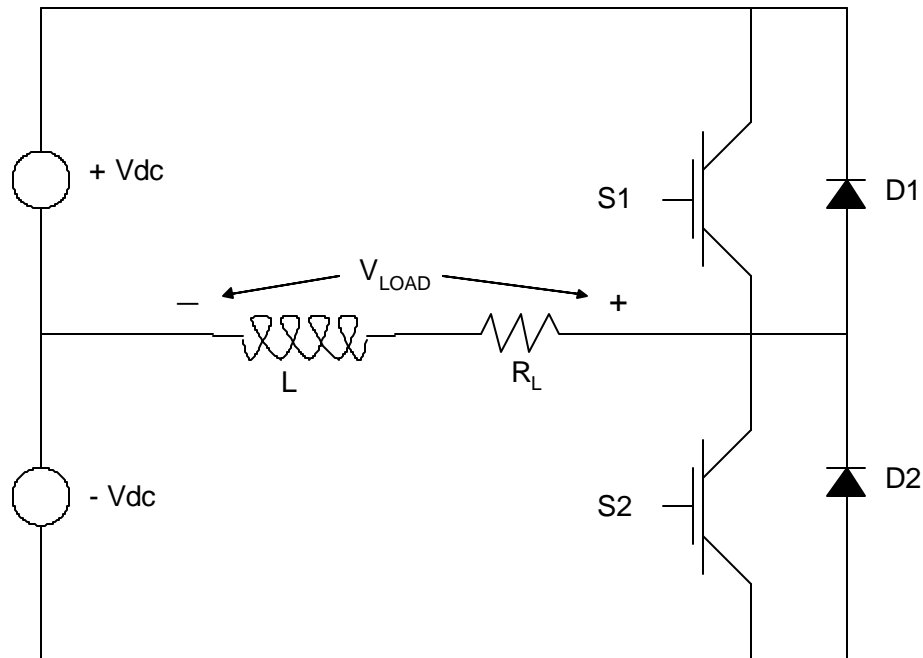


Figure 1. Half-Bridge Inverter Circuit Topology

The amplitude and frequency of the sinusoidal output of the inverter can be controlled directly by properly timing the closure and opening of switches S1

and S2. The Insulated Gate Bipolar Transistor (IGBT) is an example of a type of switch commonly used for inverters. The quality of the output waveform is dependent on a number of variables that mainly include the relative switching speed, the filtering and the bandwidth of the controller. The relative switching speed is generally specified in number of pulses (or switchings) per half-cycle of the output fundamental voltage or current [3]. For most loads, the ideal voltage and current waveforms will be sinusoidal at the desired operating frequency. For nonlinear loads, it is common to force the voltage or the current sinusoidal while letting the load characteristics define the uncontrolled variable.

Given a fixed amount of filtering and sufficient control bandwidth, the switching sequence including the relative rate at which the switches operate determines the inverter's output accuracy when following a reference sinusoid. As a result, the output of an inverter at a lower relative switching frequency will not match the desired sinusoidal pattern as closely as an inverter switching at a higher frequency. Since non-sinusoidal waveforms are rich in harmonic content that is not directly usable by a machine load, the total harmonic distortion (THD) of the current should be minimized to alleviate unwanted noise from torque pulsations and excess heating from eddy current losses.

The load current waveform, $i_L(t)$, can be represented by a composite series of the fundamental component and the sum of the higher harmonic components as shown below [3]:

$$i_L(t) = i_{L1}(t) + \sum_{h \neq 1}^{\infty} i_{Lh}(t). \quad (2-1)$$

The first term (i_{L1}) is the desired fundamental frequency component, while the summation of the i_{Lh} terms represents harmonic content. Ideally, the harmonic terms would be zero if a perfectly sinusoidal waveform at the fundamental frequency was desired. The Root-Mean-Squared (RMS) value of the current waveform is given by [3]:

$$I_L = \sqrt{I_{L1}^2 + \sum_{h \neq 1}^{\infty} I_{Lh}^2}. \quad (2-2)$$

The actual distortion present in the current waveform due to its harmonics can be derived from the above relations. The THD as a percentage of the total current waveform is given by [3]:

$$\%THD = 100 \times \sqrt{\sum_{h \neq 1}^{\infty} \left(\frac{I_{Lh}}{I_{L1}} \right)^2}. \quad (2-3)$$

The objective of the inverter system is to minimize the THD in order to match the desired reference signal as closely as possible.

Various methods can be employed to control the switches within the inverter to produce an ac output current. The objective of any switching control scheme is to sequence the switches in order to match the desired reference signal. Some switching schemes are very simple, while others are quite complex and require the use of computers and digital signal processing (DSP) equipment.

The simplest of switching methods for inverters is square-wave switching. With this method, the inverter cycles the voltage across the load by alternating the positive dc voltage and then the negative dc voltage at the desired output frequency. This method simply closes the top switch when the reference signal is positive and closes the bottom switch when the reference signal is negative. Although easy to implement, the square-wave switching method produces an output waveform that falls short of matching the sinusoidal reference signal. As a result the THD of the voltage is 47.8% and 30.5% for single-phase and three-phase, respectively [3]. The distortion in the current is based on the amount of filtering required which can be significant since the dominate harmonic is the third and fifth for single-phase and three-phase, respectively.

A more complex but commonly used switching scheme is called pulse-width modulation (PWM). PWM techniques are capable of producing a good representation of the desired waveform with only the inclusion of higher, easily filterable harmonics at the switching frequency. With PWM, the positive or negative dc input source voltage is applied to the load in pulses of varying length. While the amplitude and frequency of the pulses is fixed, the width of the individual

pulses is weighted by multiplying a reference waveform by a higher frequency triangular-carrier to produce a digitized representation of the reference.

One prevalent technique of inverter control is sine-PWM. In a sine-PWM inverter, a sinusoidal reference signal of the desired output frequency is compared to a triangular modulation signal at a much higher frequency. Figure 2 illustrates the two control signals and the switching scheme:

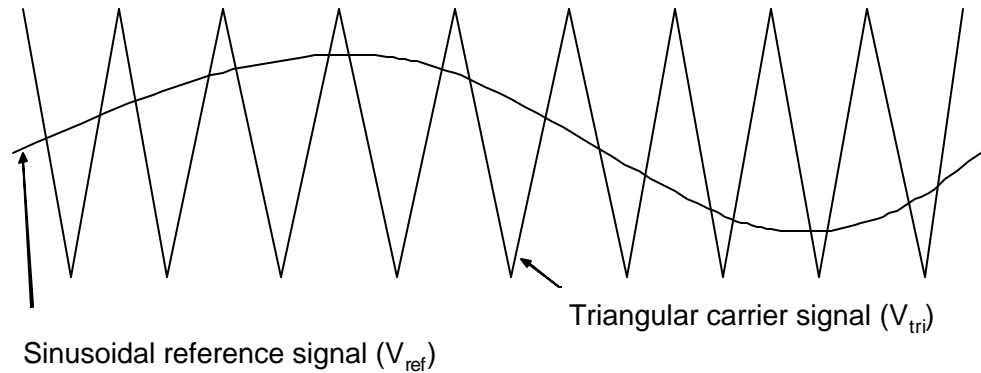


Figure 2. Pulse-width modulation reference and carrier signals

A brief description of the algorithm to control the applied voltage to the load is shown here.

- If $V_{ref} > V_{tri}$:
 - Close S1 (top switch), open S2 (bottom switch).
 - Set V_{LOAD} to $+V_{dc}$.

- If $V_{ref} < V_{tri}$:
 - Open S1 (top switch), close S2 (bottom switch)
 - Set V_{LOAD} to $-V_{dc}$

The resultant applied voltage levels for a typical cycle in a sine-PWM inverter are depicted in Figure 3.

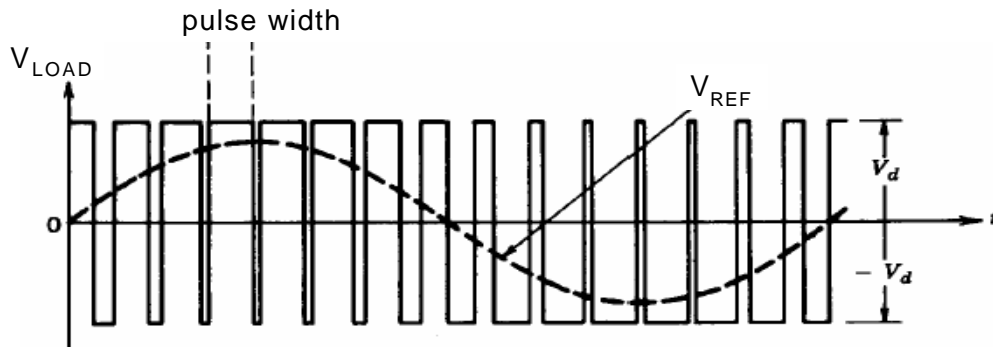


Figure 3. Typical Sine-PWM applied load voltage (From Reference 3).

This type of inverter can produce a very high fidelity current waveform and its use is widespread. The harmonic content of the current depends on the number of pulses applied per cycle. With a high integer count of pulses per half-cycle, the first non-zero harmonic present in the current waveform will be significantly separated from the fundamental and easy to filter. The order of the non-zero harmonics present are determined by

$$n = 2kr \pm 1, \quad (2-4)$$

where n represents the order of non-zero harmonics, k is the number of pulses per cycle, and r can be any positive integer. According to this relationship, a high value of k will make the minimum value of n a much higher order harmonic. For example, if there were 15 pulses per cycle in a 60-Hz waveform, then the lowest harmonic present would be the 29th harmonic ($2 \cdot 15 - 1$) at a frequency of 1740 Hz. A relatively small low-pass filter could eliminate these components from the current waveform.

Although a proven technique for inverter control, the sine-PWM switching scheme and other similar schemes have a few key disadvantages. They require the use of relatively complex hardware to implement and control, as opposed to square-wave switching which can be controlled with a simple circuit. Also, the high switching frequency often required can impose significant switching power losses as the inverter needs to switch at frequencies much higher than the fun-

damental output frequency. The higher switching frequency necessary to produce high-fidelity waveforms can often exceed the capabilities of some power electronic switches. Switches that are rated for very high voltage and current have longer delays and cannot switch as fast as lower power devices. Power electronics operating at a fixed high frequency rather than spread-spectrum may also introduce undesirable noise into the shipboard environment which could be easily detectable by the enemy.

B. HYSTERESIS CONTROL

Hysteresis control presents an alternative method for producing a sinusoidal ac current waveform from a dc voltage source. With this method, the controller maintains an output current that stays within a given tolerance of the reference waveform. The tolerance that the output stays within is called the “hysteresis band”. Unlike the above described PWM switching technique, the method of hysteresis control depends on feedback from the output current to control the inverter system. The closed-loop control method enables the inverter with hysteresis control to adapt instantly to changes in the output loading.

The concept of hysteresis control can be applied to a wide range of inverter configurations and topologies. Both single-phase and three-phase inverters can be controlled by the hysteresis method as well. A common topology for single-phase inverters is the H-bridge because it offers more controllability than the half-bridge type. It allows the use of three output states instead of two and requires half of the dc bus voltage to produce the same peak output voltage [3]. However, the minimum switch configuration and most popular topology for multi-phase inverters consists of half-bridges.

Figure 4 illustrates the fundamental concept of operation for the hysteresis-controlled inverter.

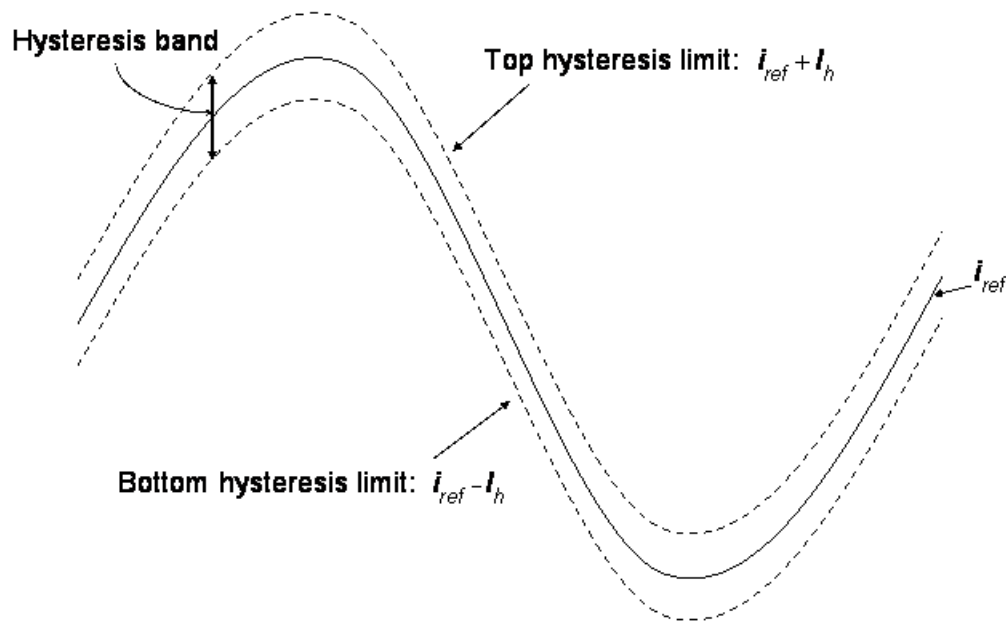


Figure 4. Hysteresis band for inverter control

The reference current, i_{ref} , represents the desired waveform for the output load current. The top and bottom hysteresis limits form the hysteresis band, which corresponds to the tolerance limit of the inverter controller. This discussion will describe a two-level hysteresis inverter switching scheme.

The two-level inverter controller will apply the positive or negative dc bus voltage to the load in order to keep the output current within the hysteresis band. For example, when the output current rises above the top hysteresis limit, the inverter controller will respond by switching the transistors to apply the negative dc bus voltage to the load and effectively reduce the value of the output current to bring it below the top hysteresis limit. The inverter controller will keep the negative dc bus voltage across the load until the output current reaches the bottom hysteresis limit. After the output current drops below the bottom limit, the inverter controller will send the appropriate gating signals to the transistors to switch them to apply the positive dc bus voltage across the load. This will bring the output current back up above the bottom hysteresis limit and within the allowable tolerance band around the reference waveform. The controller will con-

tinuously repeat this cycle to maintain the output load current within the hysteresis band.

Unlike other high-fidelity inverter control strategies, the hysteresis controller will operate at a variable switching frequency that is spread across the spectrum. The instantaneous switching frequency f_s at any point on the current waveform can be predicted by [3]:

$$f_s = \frac{(V_{dc} - |i_{ref}|) |i_{ref}|}{L I_h V_{dc}}, \quad (2-5)$$

where V_{dc} is the dc bus voltage, i_{ref} is the instantaneous voltage of reference current signal, L is the load inductance, and I_h is the width of the hysteresis band.

As reflected in Equation 2-5, the hysteresis inverter will switch faster at points in the cycle where the reference current reaches its maximum and minimum values and switch much slower when i_{ref} is close to zero in magnitude. A larger load inductance will allow the inverter to switch at a lower frequency to maintain the current within the same hysteresis band. Since f_s will diverge to infinity if L is equal to zero, there must be some inductance present in the load for the hysteresis-controlled inverter to work. The switching frequency is also inversely proportional to I_h . The inverter will switch at higher rates overall to achieve a higher fidelity output current within a smaller hysteresis band.

C. HYBRID INVERTERS

All of the above described switching schemes have distinct advantages and disadvantages in their design. In general, a more complex switching scheme such as sine-PWM will produce a more sinusoidal waveform, but it will incur a larger power loss in the switching states as it must switch at a higher rate. Also, a higher switching frequency may mandate the use of higher speed switches which cannot handle as much current and voltage. In order to produce higher power, slower switching is required given the same system components.

Conversely, the simple bulk converter arrangement only switches at a rate equal to the actual output waveform and therefore incurs much lower overall

switching losses. Since the bulk converter does not switch at a very high frequency, it can exploit the high power capability of the Gate Turn-Off thyristor (GTO) or its derivatives for high voltage and current operation. However, the output waveform of this type of inverter is too rich in harmonic content for military propulsion loads and may not fit the requirements of many types of ancillary ac loads. Most motor drives need a relatively smooth, sinusoidal input current to operate properly without derating.

Recent research efforts have explored many different options in creating hybrid inverters to capitalize on the advantages of each switching strategy. Each effort concentrates on the common goal of producing the highest possible quality of output waveform that can supply the maximum amount of power. The new inverter control strategies also aim to add flexibility, reliability, and simplicity to the process of converting dc to ac power.

One novel control strategy created a hybrid inverter from a high-fidelity IGBT-based inverter and a low-fidelity GTO-based inverter. The complete details of this system can be found in Reference 4. This hybrid system used a common dc source voltage for the two series-connected three-phase inverters. The topology of the system is depicted in Figure 5.

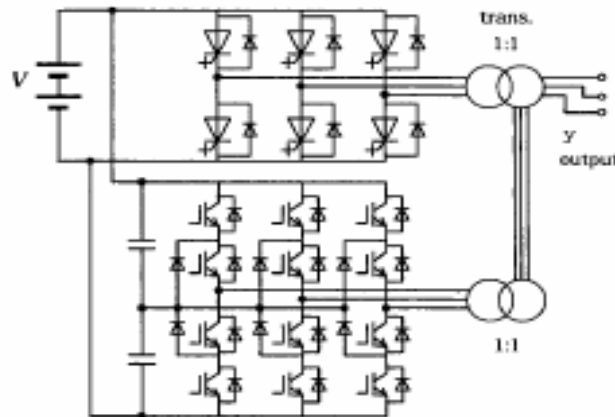


Figure 5. Topology of series-connected hybrid inverter (from Reference 2).

The bulk inverter, with GTO switches operating at the low load frequency, produced the majority (up to 63.7%) of the output power. The high-fidelity IGBT-

based inverter created the remainder of the power at the fundamental output frequency and worked to offset the lower order harmonics produced by the bulk inverter. This hybrid inverter strategy worked well in practical experimentation as the output from the series-connected inverters had a current THD of only 1.96% due to the suppression of harmonics by the IGBT-based inverter.

A separate research effort, described in Reference 5, also explored the concept of a hybrid inverter system with favorable results [5]. This experiment placed a current-source inverter operating in a square-wave mode in parallel with a high fidelity voltage-source inverter switching in a PWM mode at a much higher frequency. The topology of this hybrid inverter system appears below.

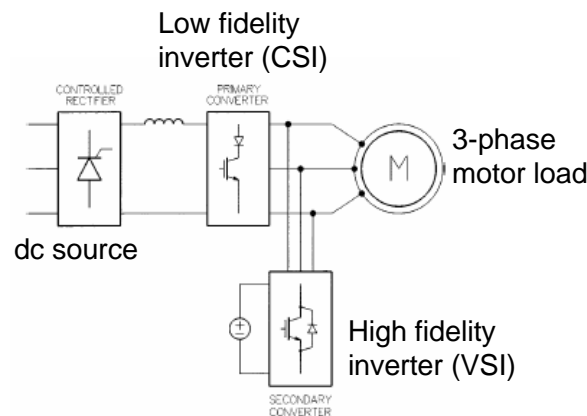


Figure 6. Hybrid current-source/voltage source inverter (From Reference 5).

This system used the primary low fidelity inverter to generate the bulk of the current while the secondary high fidelity inverter cancels out the low order harmonics of the primary inverter output and augments the output at the desired fundamental frequency. The experimental results for this system proved that it could offer improved efficiency and responsiveness while minimizing switching losses.

Although both of the above described research efforts proved the concept of a square-wave mode inverter coupled with a high-fidelity inverter, they both require the use of a complex computer system to control the switching cycles. A

DSP system metered the gating signals to the high fidelity PWM inverter in both cases.

The basics of inverters were introduced in this chapter as well as some prevalent switching schemes. A survey of current research pointed out the emerging technology in hybrid inverter systems. This thesis will propose a distinct alternative to these hybrid inverter systems that relies only on simple discrete circuits to control the inverter switches and does not require the use of complex DSP equipment. The system proposed in this thesis will couple a simple six-step bulk inverter in parallel with a high-fidelity inverter which employs the novel, yet simple concept of hysteresis control. The following chapter will detail the design and development of this hybrid inverter system.

THIS PAGE INTENTIONALLY LEFT BLANK

III. SYSTEM DESIGN AND DEVELOPMENT

The hybrid inverter system brings several elements together to produce its output current for the load. The design and construction of the complete inverter as well as the component subsystems will be described in this chapter.

A. OVERALL SYSTEM DESIGN

The hybrid inverter system combines a relatively simple six-step bulk inverter and a high fidelity hysteresis controlled inverter to create a three-phase, sinusoidal output current at the desired magnitude and frequency. The objective of the inverter is to match a given reference current signal as closely as possible with the output load current for each phase.

The bulk inverter utilizes a simple switching scheme to produce a three-phase, six-step output voltage across the load at the fundamental frequency. Since it switches at low frequency, the bulk inverter incurs only minimal switching power losses compared to a higher fidelity inverter that switches at a much higher rate.

The hysteresis inverter is connected in parallel with the bulk inverter and utilizes the same dc power source. The high fidelity inverter with a closed current-control loop serves to cancel the harmonics of the bulk inverter and make the resultant sum of the two currents match the desired reference current across the load. The load current for each phase complies with the following relation:

$$i_L(t) = i_B(t) + i_H(t), \quad (3-1)$$

where i_B represents the bulk inverter output current and i_H denotes the current component produced by the hysteresis inverter. The hysteresis inverter monitors the instantaneous value of the load current, i_L , and adjusts the output current of each phase to match the desired reference signal. The addition of the hysteresis inverter enables the composite hybrid system to continuously adapt to changes in the load current and effectively closes the current control loop. The system level block diagram is depicted in Figure 7.

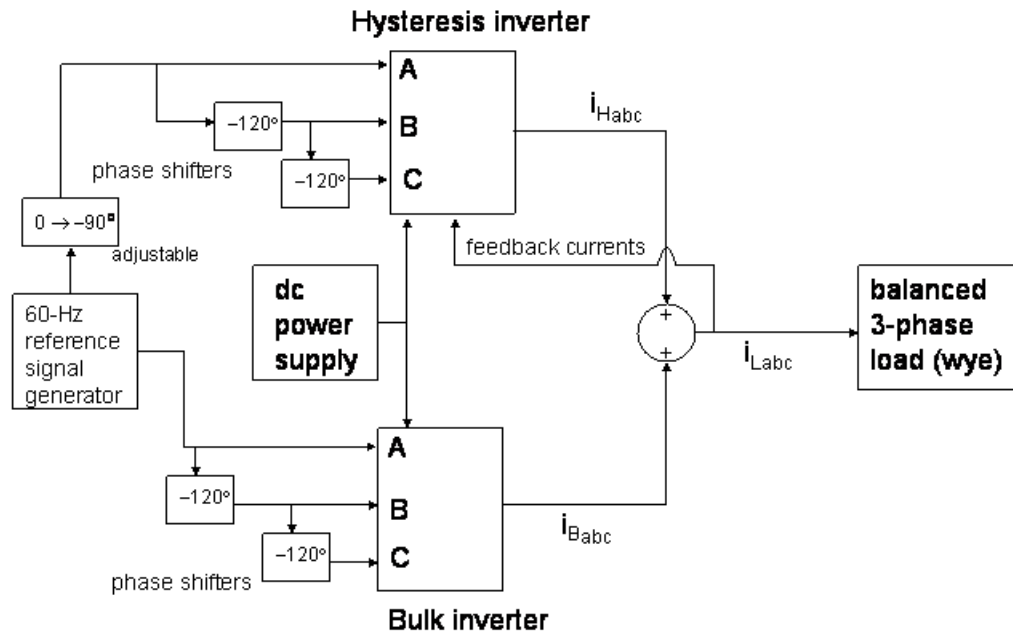


Figure 7. Overall system block diagram of hybrid inverter system.

The reference signals for each phase current come from a common signal generator, which utilizes a simple oscillator to produce a sinusoid at the desired frequency of 60 Hz. This signal passes through subsequent all-pass filters that create the 120 degrees of phase separation for phases A, B, and C. Also, the overall phase shift between the hysteresis inverter reference signal and the bulk inverter reference signal can be changed with an adjustable phase-shifter. The phase-shift between the two inverter elements can be tuned to optimize the hybrid inverter system. The following sections will discuss the details of each element of the system.

B. HYSTERESIS INVERTER

The hybrid inverter utilizes the hysteresis inverter that was developed and tested with good results in a previous research effort. It is a closed-loop Current Source Inverter (CSI). The complete results of the testing and details of the design process can be found in Reference 2. The hysteresis inverter consists of a controller section and a power section. The controller section generates logic signals to the transistor switches and controls the output current to keep it within a desired tolerance band based on the reference current signal. The power sec-

tion takes the logic signal output of the controller section and amplifies them into switching signals to the six IGBT switches of the inverter. The power section is a half-bridge type configuration with an upper and lower switch for each phase. The schematic diagrams for both the controller section and the power section appear below in Figures 8 and 9, respectively.

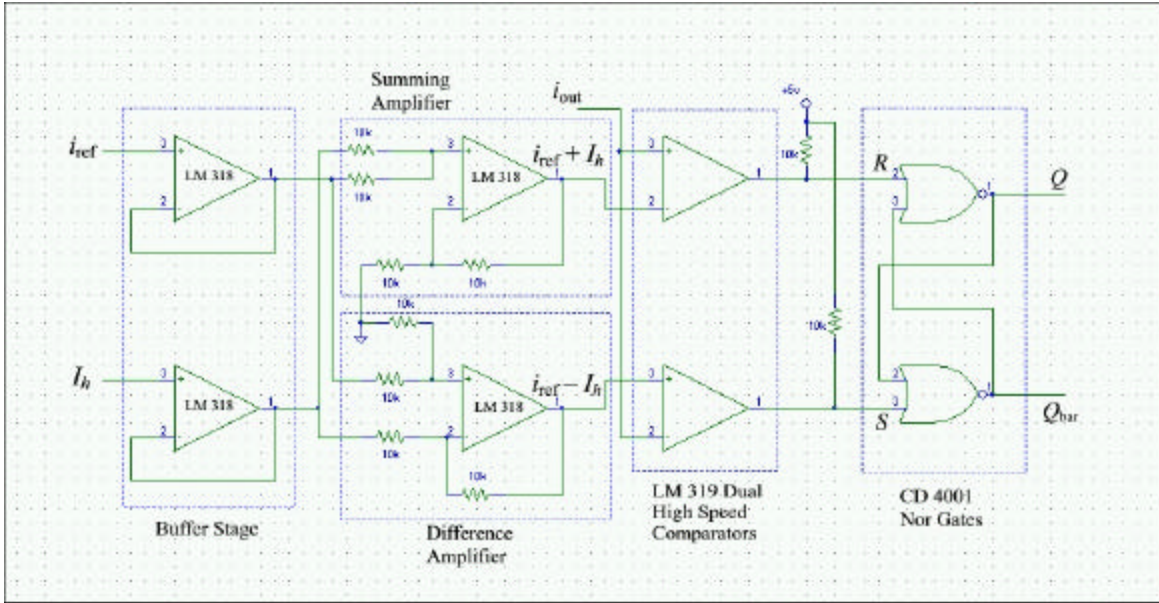


Figure 8. Controller section of hysteresis inverter (From Reference 2).

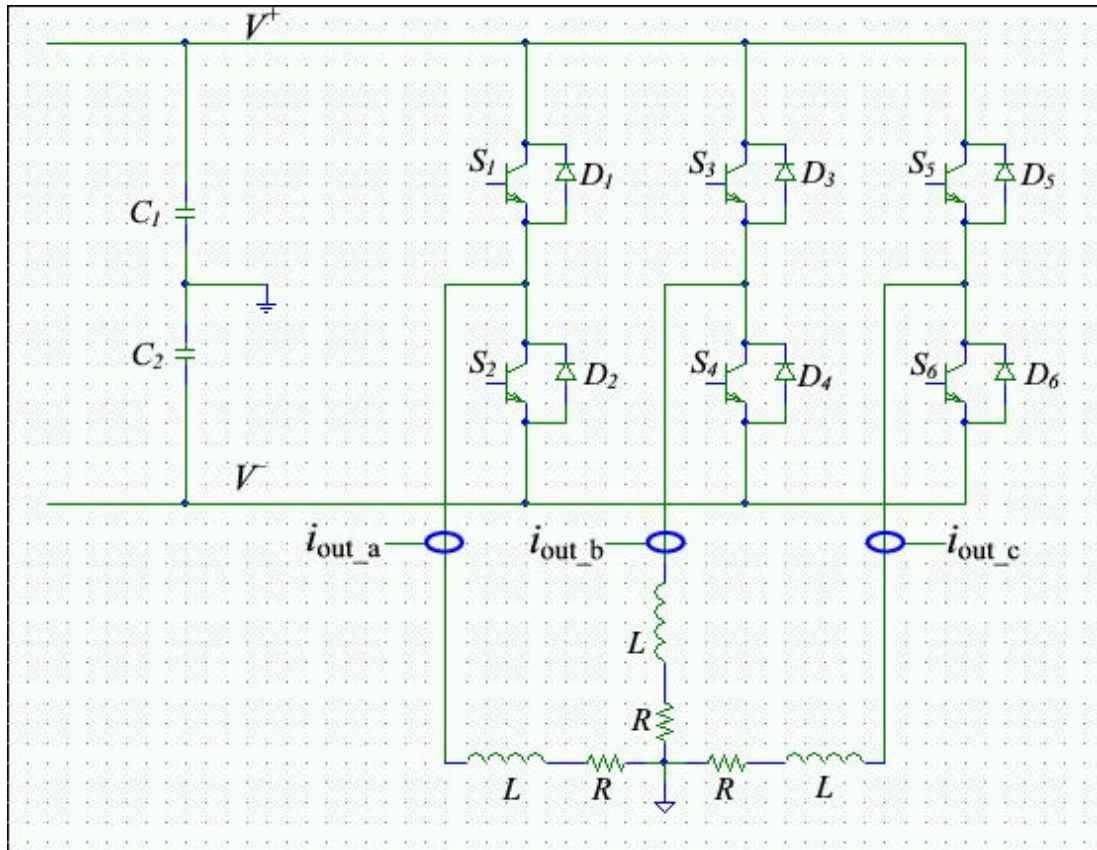


Figure 9. Power section of hysteresis inverter (From Reference 2).

The hysteresis inverter viewed as a subsystem is represented in the block diagram in Figure 10 below.

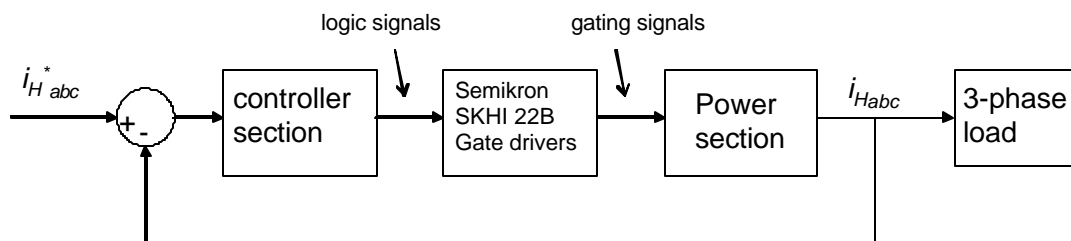


Figure 10. Block diagram of hysteresis inverter (After Reference 2).

The block diagram in Figure 10 shows that the hysteresis inverter provides the unique advantage of a closed-loop system for the control of the load current. The closed-loop control will provide the key to the successful operation of the

entire system when paralleled with the bulk inverter described in the following sections.

C. BULK INVERTER

The bulk inverter produces a three-phase, six-step output to supply the majority of the current at the fundamental frequency in the overall system. It is an open-loop Voltage Source Inverter (VSI). The bulk inverter also provides the reference current signal for the hysteresis inverter controller.

Constructed from discrete components, the bulk inverter consists of several elements that work in concert to create a three-phase output. The system block diagram for the bulk inverter controller is depicted in Figure 11. The three voltage reference signals that appear in the figure are used to determine cross-over points by the comparator circuit.

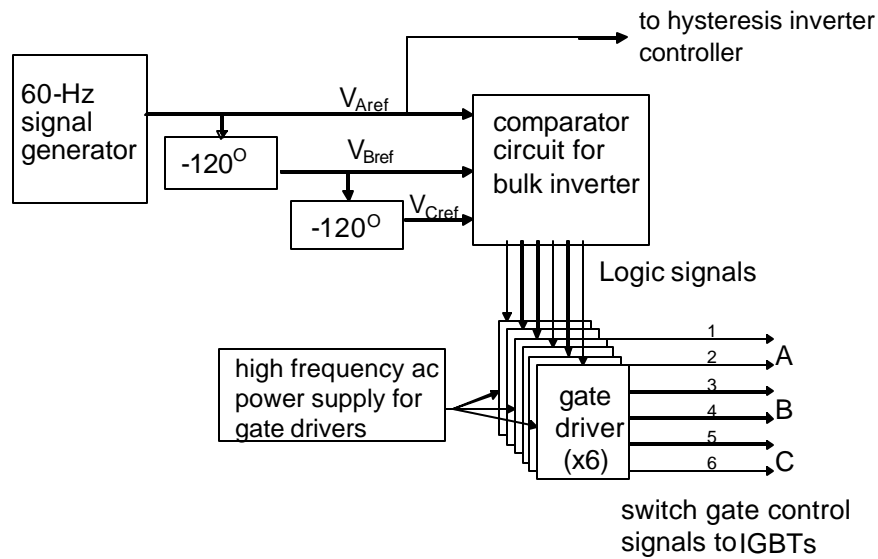


Figure 11. System block diagram of bulk inverter controller.

The timing of the switches in the bulk inverter and the reference current waveform for the hysteresis inverter both come from the same 60-Hz oscillator. The schematic diagram in Figure 12 shows the simple design used to realize the oscillator.

This circuit produces a steady sinusoidal signal at a frequency of 60 Hz with an amplitude of 10 V peak. The output of the oscillator serves as phase A of

the inverters. To create the other two phases of the inverters, the phase A signal is shifted by 120° sequentially to produce phases B and C. The phase-shifter circuit used appears in Figure 13.

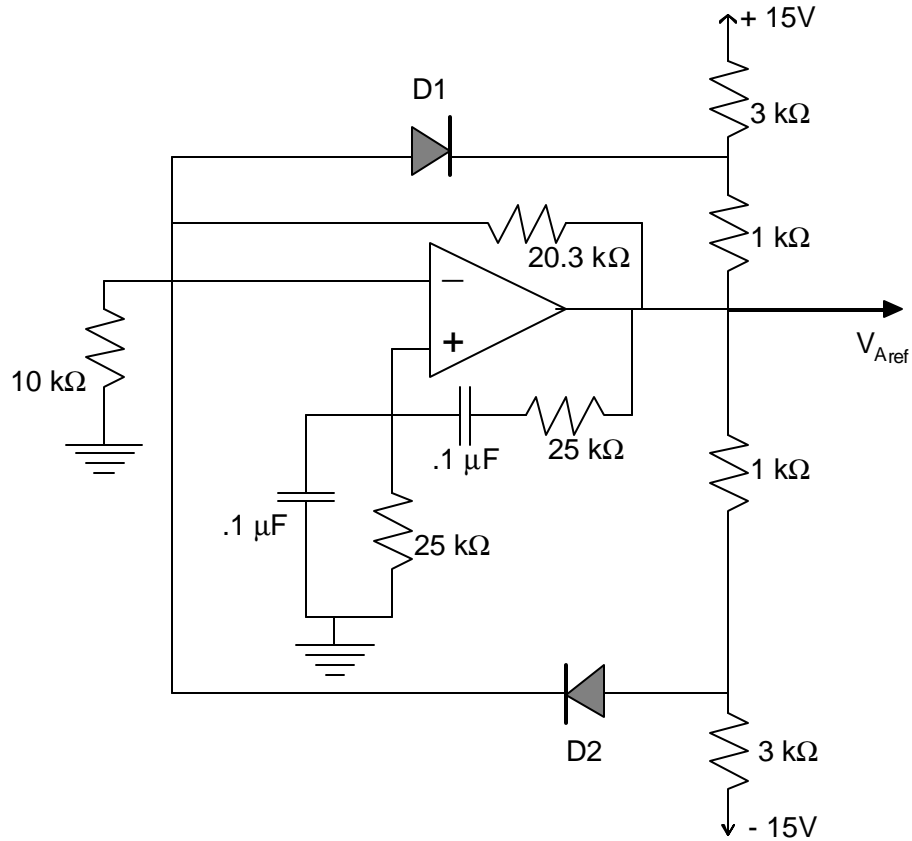


Figure 12. 60-Hz signal generator circuit (After Reference 6).

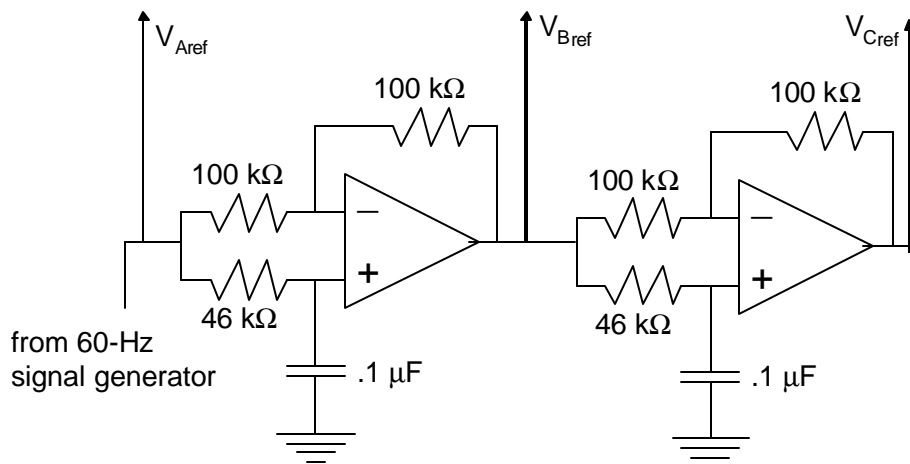


Figure 13. Phase-shifter circuit (After Reference 7).

In order to control the switches for each of the three phases of the bulk inverter, the sinusoidal reference signals pass through a network of comparator circuits. Based on the LM311 comparator, these circuits take the reference signal input and produce square-wave pulse signals to the upper and lower switches of the bulk inverter. This network is shown in Figure 14. The reference signal labeled as V_{ref} represents any of the three phase reference signals (V_{Aref} , V_{Bref} , or V_{Cref}) depicted in Figure 13. The top comparator circuit will send a gate signal of +15 V to the upper switch when the reference signal exceeds a threshold of 2.5 V. Therefore, the comparator will generate a positive voltage signal for most of the positive half cycle of that particular phase. The other comparator on the bottom will correspondingly send a positive logic signal to the lower switch when the reference voltage falls below -2.5 V. A small hysteresis current through the positive feedback loop ensures that the output does not oscillate at the transitions. The threshold for the logic signal switching was set to 2.5 V to guarantee that an upper and lower switch in the same phase-leg are not activated simultaneously.

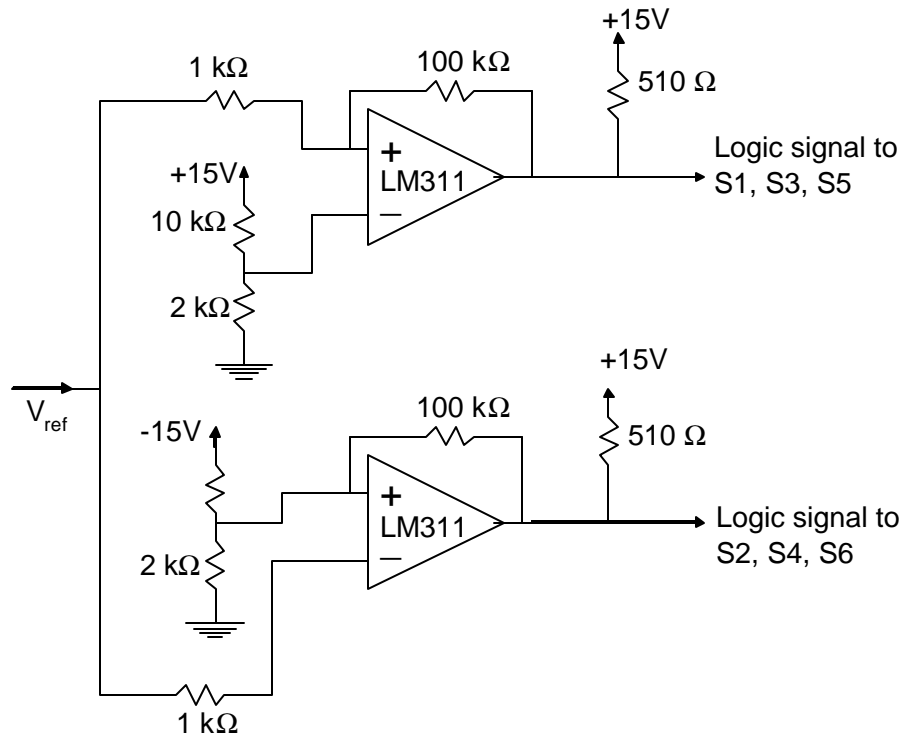


Figure 14. Comparator circuit to generate logic signals to switches.

The controller for the bulk inverter also serves as the reference signal source for the hysteresis inverter. The same signal that generates the logic signals to phase A of the bulk inverter drives the timing of the hysteresis inverter. After it leaves the bulk inverter controller, the current reference signal passes through a basic amplifier that sets the desired magnitude of the output load current. The signal then passes through a phase-shifter that can set the overall phase shift between the reference signal and the bulk inverter phase voltage. This signal then goes into the hysteresis inverter as the phase A current reference signal. A pair of phase-shifters identical to those depicted in Figure 13 generates the reference current signals for phases B and C of the hysteresis inverter. Figure 15 shows the schematic diagram for this hysteresis signal reference circuit.

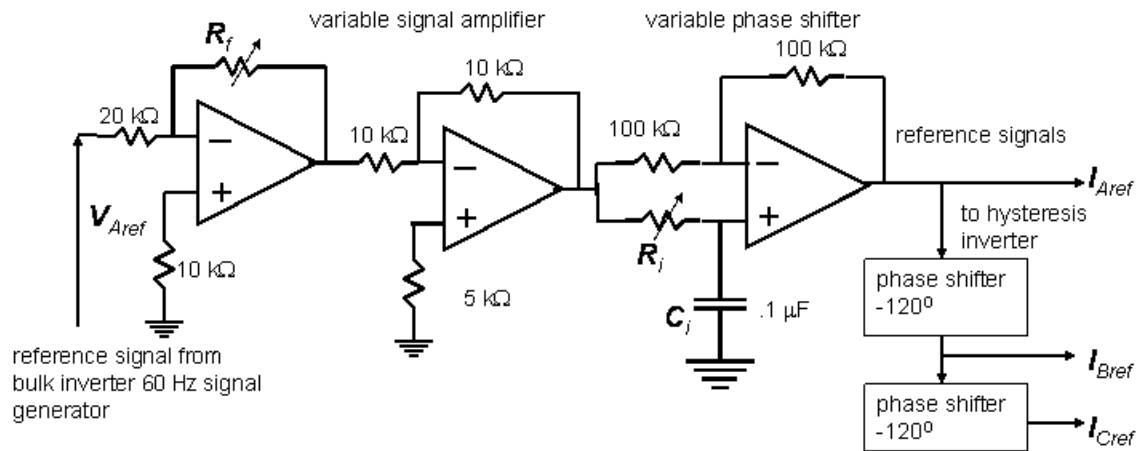


Figure 15. Hysteresis signal reference circuit.

In the configuration above, the first-stage amplifier has a variable resistor in the feedback loop labeled as R_f . The desired magnitude of the reference current signal to the hysteresis inverter can be set by adjusting the value of R_f . The value of the input resistor is fixed at 20 k Ω and the amplitude of the reference signal input is 10 V. The magnitude of the current reference signal, I_{ref} , complies with the following equation:

$$I_{ref} = \frac{10R_f}{20 \times 10^3} = \frac{R_f}{2000}. \quad (3-2)$$

The actual reference current signal will follow a 1:1 relationship with the voltage signal I_{ref} in Equation 3-2. In the experimental configuration studied, the value of R_f is 10 k Ω to reduce the magnitude of the reference signal I_{ref} to 5 V. This commands the hysteresis inverter controller to maintain the load current amplitude at 5 A.

The phase shift of the reference current relative to the bulk inverter phase voltage will depend on the value of R_i in the variable phase shifter depicted in Figure 15. For this application, the value of R_i was varied using a 0–100 k Ω potentiometer. Following the same principles as the phase shifter circuits in Figure 13, the amount of phase shift depends on the RC time constant of the circuit and the input frequency, f , as illustrated by [7]:

$$f = 2 \tan^{-1}(2\pi f R_i C_i). \quad (3-3)$$

With the capacitance C_i held constant and f set at 60 Hz, the variable resistance R_i can be adjusted with the potentiometer to obtain the desired phase shift.

The circuits depicted above were built from discrete components on common wire-wrap breadboard. A printed circuit board with copper on both sides surrounded the circuit and supported a common ground plane, a positive supply input, a negative supply input, and connections for the system outputs. Tables contained in Appendix A list the specific pin connections of the components.

From the comparator circuit (Figure 14), the logic output signal passes into the gate driver circuit (Figure 17). This circuit converts a logic signal into an appropriate level to properly gate an IGBT in the bulk inverter power section; a Toshiba TLP250 photocoupler is the main component. The gate driver circuit is also necessary for providing electrical isolation. The control circuitry must be isolated from the high voltage and current associated with actual inverter switches. Further, isolation is necessary between individual switches. Reference 8 provides a more detailed description of the gate driver circuit.

An amplified square wave input provides the basic power to the TLP250 via a high-frequency transformer (Magnetek GDE25-2) and a full-bridge rectifier (using four 1N4148 fast-recovery diodes). A common amplifier supplied the power for all six gate driver circuits. A function generator set at 20 kHz was used for the input to the amplifier. A 1- μF capacitor filters out high frequency noise at the output of the circuit to ensure that only the low frequency switching signal gets to the transistors. The circuit diagrams for the signal amplifier and the gate driver circuit are depicted below in Figures 16 and 17, respectively.

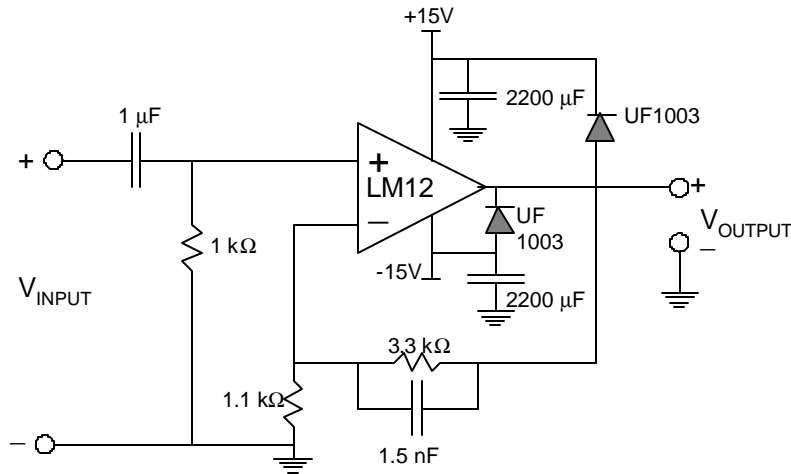


Figure 16. Amplifier circuit for square wave signal.

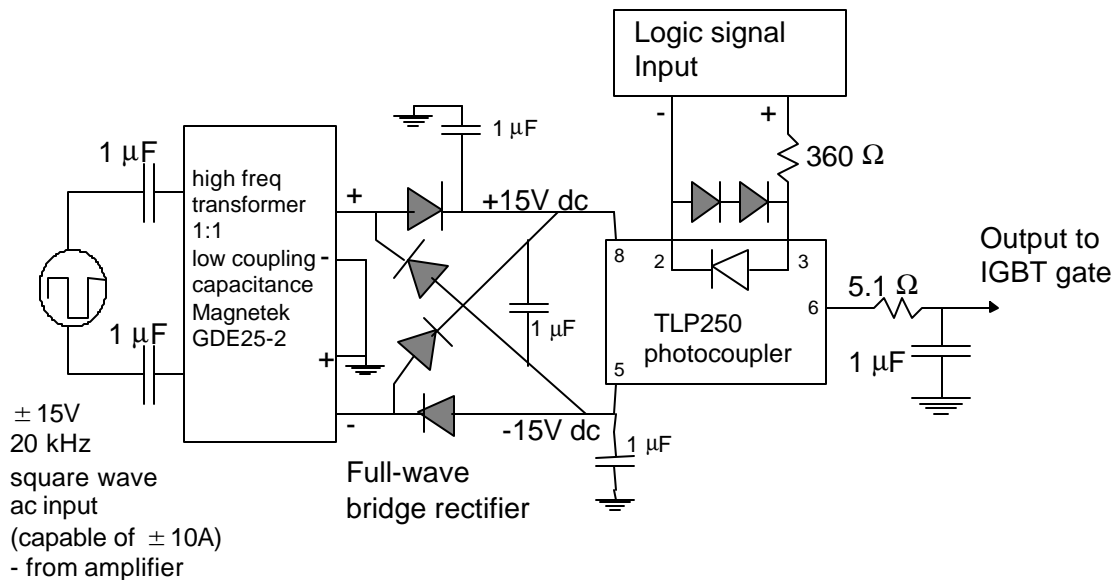


Figure 17. Gate Driver Circuit (After Reference 8).

The six identical gate driver circuits supplied the triggering signals to the six bulk inverter IGBTs to produce an alternating current. The transistor switches utilized were the Toshiba MG50Q2YS9 which combined the upper and lower switches and diodes for each phase in the same package. Each switch is rated for $V_{CE} = 1200 \text{ V}$ and $I_C = 50 \text{ A}$. The total switching delay time for the IGBT is calculated below.

$$t_{on} = t_{d(on)} + t_r, \quad (3-4)$$

and

$$t_{off} = t_{d(off)} + t_f, \quad (3-5)$$

where $t_{d(on)} = 0.8 \mu\text{s}$, $t_r = 0.6 \mu\text{s}$, $t_{d(off)} = 1.8 \mu\text{s}$, and $t_f = 1.0 \mu\text{s}$ [9].

From the data presented above, the total time required to turn the IGBT on is $1.4 \mu\text{s}$ and the total time to turn it off is $2.8 \mu\text{s}$. Therefore, the total switching delay for each cycle is $4.2 \mu\text{s}$. The maximum allowable switching frequency of the transistor can then be computed as:

$$f_{\max} = \frac{1}{t_{on} + t_{off}} = \frac{1}{4.2 \text{ } \mu\text{s}} = 238.1 \text{ kHz}. \quad (3-6)$$

The actual delay of the IGBT used is insignificant when coupled with the gate driver circuit used in this inverter. The measured delays are $100 \mu\text{s}$ and $90 \mu\text{s}$ for turn-on and turn-off, respectively. Therefore, the total delay of $190 \mu\text{s}$ far exceeds the IGBT switching time of $4.2 \mu\text{s}$. Given the above delay, the maximum operation frequency drops to 5.2 kHz . Since each switch in the power section of the bulk inverter will only turn on and off at a rate of 60 Hz , this frequency limitation is not an issue.

D. SYSTEM CONFIGURATION

As configured in Figure 18, the bulk and hysteresis inverters are combined via inductors prior to the load. Ideally, the bulk inverter will provide all of the required current at the fundamental frequency of 60 Hz while the hysteresis inverter will add the current components necessary to cancel harmonics in order to shape the waveform to match the reference signal. The closed-loop system pro-

vided by the hysteresis inverter will continuously adjust the load current within the tolerance band to ensure that it stays at the desired level.

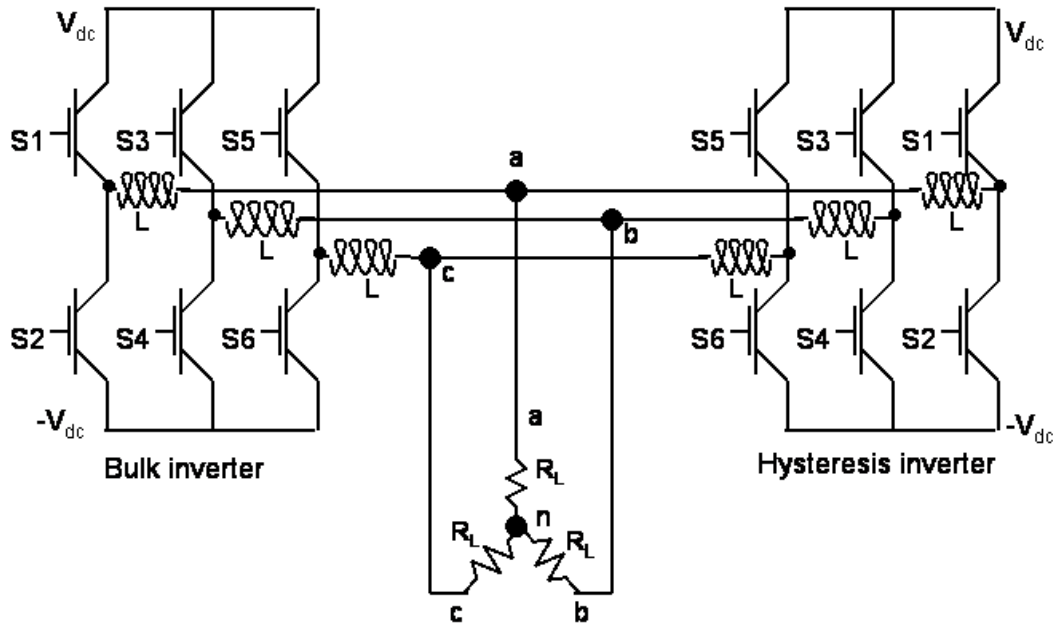


Figure 18. Power section topology of hybrid inverter.

In Figure 18, the two inverters are connected in parallel to drive a common three-phase wye-connected resistive load. Although this diagram depicts a purely resistive common load, the hybrid inverter can drive a load with a lagging power factor as well. In the experimental testing of the system, the value of R_L is 1.05Ω and the inductances L are 9.1 mH .

The detailed designs of the components that comprise the hybrid inverter were presented in this chapter. The design of the hysteresis inverter element was described as well as the fabrication of the six-step bulk inverter control circuits and power section. The following chapter will expand on the theoretical predictions for the system performance and simulate the operation of the newly constructed bulk inverter.

IV. THEORETICAL RESULTS

The hybrid inverter system combines two predictable elements to form a unique composite topology to produce ac power. This chapter presents the theory behind their operation.

A. OVERALL PERFORMANCE

The requisite load of the hybrid inverter consists of an inductive element and a resistive element. In the configuration studied, the output of each inverter is connected to a separate inductor that feeds current into a parallel-connected load. A model of the topology used in this experiment is depicted in Figure 19 below. The figure depicts the combined phase A of the parallel-connected inverters. The topology for phases B and C are identical.

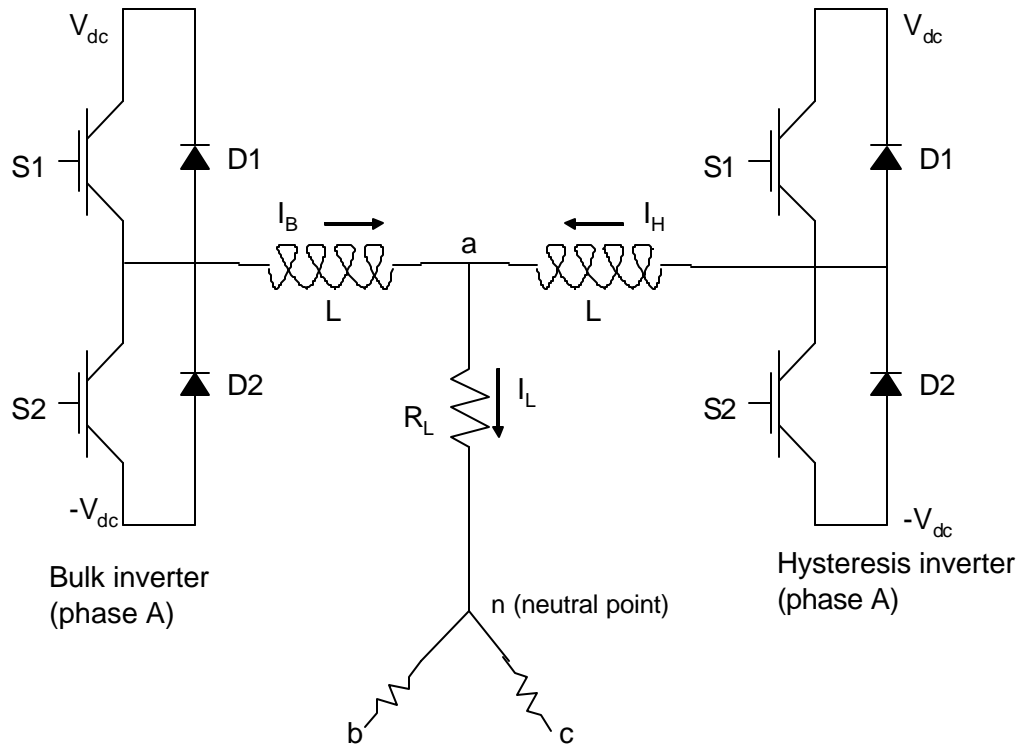


Figure 19. Topology of single phase of hybrid inverter.

As discussed in the previous chapter, the load current consists of the sum of the output currents of the bulk and hysteresis inverter sections. The induct-

ances on the output of each inverter are of equal value and they are connected to a three-phase, balanced resistive load. The neutral point is floating in this configuration. In order to evaluate the resultant load current, i_L , the current components produced by each inverter section are computed individually. By the principle of superposition, the hysteresis inverter is replaced with an open circuit and the load current produced by the bulk inverter is computed. Similarly, the bulk inverter is replaced by an open circuit while the hysteresis inverter current is quantified. The total load current is found by simply adding the two separate current components coming into the node at point “a”.

B. HYSTERESIS INVERTER CURRENT

The current produced by the hysteresis inverter follows the model developed in Reference 2. Utilizing two-level switching, the hysteresis inverter applies either $+V_{dc}$ or $-V_{dc}$ across the load. Therefore, two simple equations describe the current across the load for each case. For the case where the positive dc voltage is applied, the load current complies with [2]

$$i_L(t) = e^{\frac{-R}{L}(t-t_0)} i_L(t_0) + \frac{V_{dc}}{R} \left(1 - e^{\frac{-R}{L}(t-t_0)} \right). \quad (4-1)$$

When the hysteresis inverter applies the negative dc voltage to the load, the negative sign appears in front of the V_{dc} term in Equation 4-1 and the current is described by [2]

$$i_L(t) = e^{\frac{-R}{L}(t-t_0)} i_L(t_0) + \frac{-V_{dc}}{R} \left(1 - e^{\frac{-R}{L}(t-t_0)} \right). \quad (4-2)$$

The above set of equations show that there must be an appropriate amount of inductance L in the circuit in order to prevent the load current from changing instantaneously. It also indicates that larger time constants will slow the rate of change of the current. This translates to a slower rate of switching for the controller given a fixed hysteresis band and bus voltage. Since L is generally fixed, the load range for optimal operation of the converter will be restricted. The predicted switching frequency can be computed from the system parameters using Equation 2-5 as discussed earlier in the thesis.

C. BULK INVERTER CURRENT

Contrary to the hysteresis inverter, the applied voltage of the bulk inverter follows a prescribed pattern with six discrete steps in each cycle. Each phase voltage waveform is separated by a phase shift of 120° from the other two phases. The voltages applied to the load depend only on the dc bus voltage and there is no feedback input from the inverter output.

Figure 20 depicts the voltage steps of phase A for one period of a reference 60-Hz sine wave. The bulk inverter produces a quantized representation of the sinusoidal reference signal. On the y-axis labels of Figure 20, the quantity ΔV_{dc} is defined by the total voltage across the dc bus from $+V_{dc}$ to $-V_{dc}$. If the positive and negative bus voltages are equal in magnitude, then the value of ΔV_{dc} would be equal to $2V_{dc}$. Since there are only four possible voltage levels, the bulk inverter produces a relatively rough approximation of the desired sinusoidal waveform and will generate considerable harmonic content above the fundamental frequency.

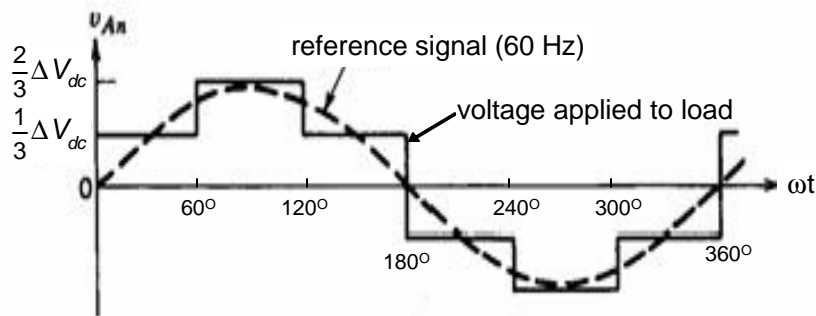


Figure 20. Phase A applied voltage for bulk inverter (From Reference 3).

To produce the various steps throughout the cycle on the phase voltage waveform, the bulk inverter opens and closes each of the six switches in the power section in a specified pattern. Each switch is closed for 180° out of the 360° cycle and open for the remainder. The prescribed switching algorithm for

the six-step bulk inverter is listed in Table 1 below. Refer to the bulk inverter topology diagram in Figure 18 for the position of the inverter switches 1-6.

Interval (degrees)	Switch state					
	Switch 1	Switch 2	Switch 3	Switch 4	Switch 5	Switch 6
0-60	closed	open	open	closed	closed	open
60-120	closed	open	open	closed	open	closed
120-180	closed	open	closed	open	open	closed
180-240	open	closed	closed	open	open	closed
240-300	open	closed	closed	open	closed	open
300-360	open	closed	open	closed	closed	open

Table 1. Switching algorithm for six-step bulk inverter.

The rate of change of the current varies as the voltage applied across the load steps through each discrete level. With a purely resistive load, the current waveform matches the voltage waveform. However, the addition of inductive elements in the load makes the current waveform lag behind the voltage waveform in the time domain. For phase A, the current across the load complies with the following relation:

$$i_{La}(t) = e^{\frac{-R}{L}(t-t_0)} i_{La}(t_0) + \frac{V_{an}(t)}{R} \left(1 - e^{\frac{-R}{L}(t-t_0)} \right). \quad (4-3)$$

In Equation 4-3, the initial conditions, t_0 and $i_{La}(t_0)$, are reset to the instantaneous value when a switching event occurs during the cycle and the phase voltage, $V_{an}(t)$, steps to the next value. For example, if $V_{an}(t)$ doubles in magnitude from $\frac{1}{2} DV_{dc}$ to DV_{dc} at time $t = 2.8$ ms, then the value of t_0 would become 2.8 ms and the new value of $i_{La}(t_0)$ would be the magnitude of the phase A load current at that time. The current follows the simple exponential relation in Equation 4-3

with these initial conditions and a constant applied voltage until the voltage steps to the next value 2.8 ms later. With a 60-Hz fundamental frequency, a switching event occurs every 2.8 ms, which corresponds to a change of $\omega t = 60^\circ$, a product of frequency and time.

Similar to the relationship described for phase A, the load currents for the bulk inverter for phase B and phase C are quantified by

$$i_{Lb}(t) = e^{\frac{-R}{L}(t-t_0)} i_{Lb}(t_0) + \frac{V_{bn}(t)}{R} \left(1 - e^{\frac{-R}{L}(t-t_0)} \right). \quad (4-4)$$

$$i_{Lc}(t) = e^{\frac{-R}{L}(t-t_0)} i_{Lc}(t_0) + \frac{V_{cn}(t)}{R} \left(1 - e^{\frac{-R}{L}(t-t_0)} \right). \quad (4-5)$$

The above equations form the basis of the simulation created to model the load current generated by the bulk inverter. A MATLAB script file was used to plot the expected load current and voltage for the bulk inverter with an applied dc bus of 39 V and a load of 1.05 Ω in series with 9.1 mH for each phase. Appendix B contains the MATLAB code for the simulation. The phase current and voltage for the bulk inverter appear in Figure 21.

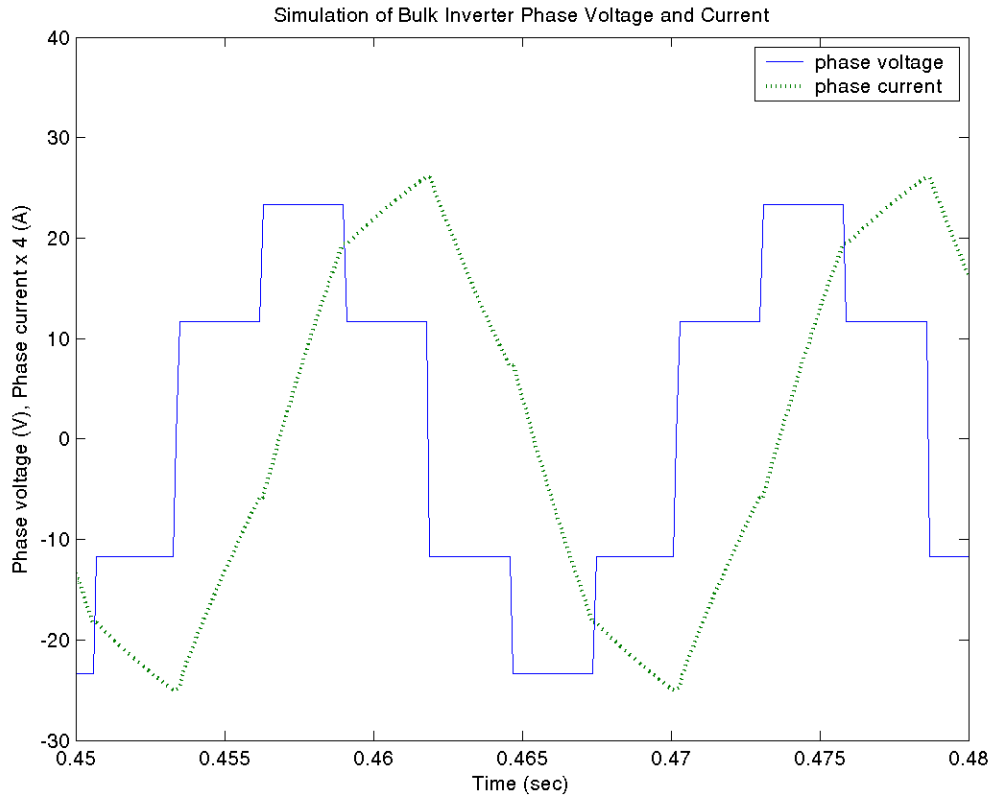


Figure 21. Results of simulation of bulk inverter, phase A.

In the simulation of the bulk inverter, the phase A voltage followed the six-step pattern described earlier. With a total applied dc bus voltage of 39 V, the phase A voltage stepped through the discrete levels of 12 V, 24 V, -12 V, and -24 V to approximate a sinusoidal reference signal. The simulation accounted for a voltage drop of 2 V across each switch as specified on the data sheet for the IGBT used [9].

The phase A load current in Figure 21 is scaled by a factor of 4 to amplify the waveform with respect to the phase voltage. From Figure 21, the phase A current lags behind the phase A voltage by 3.5 ms. At a frequency of 60 Hz, the time delay of 3.5 ms corresponds to a phase shift of -75° . The large phase shift reflects the heavily inductive load in the simulated circuit. The angle of the phase shift depends on the characteristics of the load and is computed by:

$$q_n = \cos^{-1} \left(\frac{R}{|Z_n|} \right), \quad (4-6)$$

where q_n is the phase shift at harmonic number n and Z_n is the total impedance at the n^{th} harmonic.

The magnitude of Z_n can be calculated from the resistance and reactance components of the load as follows:

$$|Z_n| = \sqrt{R^2 + (jn\omega_1 L)^2}, \quad (4-7)$$

where R is the load resistance, ω_1 represents the fundamental frequency, and L is the load inductance. Consisting of a 9.1 mH inductor coupled with a 1.05 Ω resistor, the load in the circuit has an angle of 73° at the fundamental frequency of 60 Hz ($n=1$). The higher harmonic components will have different total impedances and, therefore, they will be shifted in phase to a greater extent. The actual current waveform for the bulk inverter will lag behind the voltage by a phase shift greater than 73° due to its significant harmonic content. As a result, the simulation produced a larger phase shift of 75° .

Figure 22 shows a detailed view of the three phase currents in the time domain for the bulk inverter operating independently.

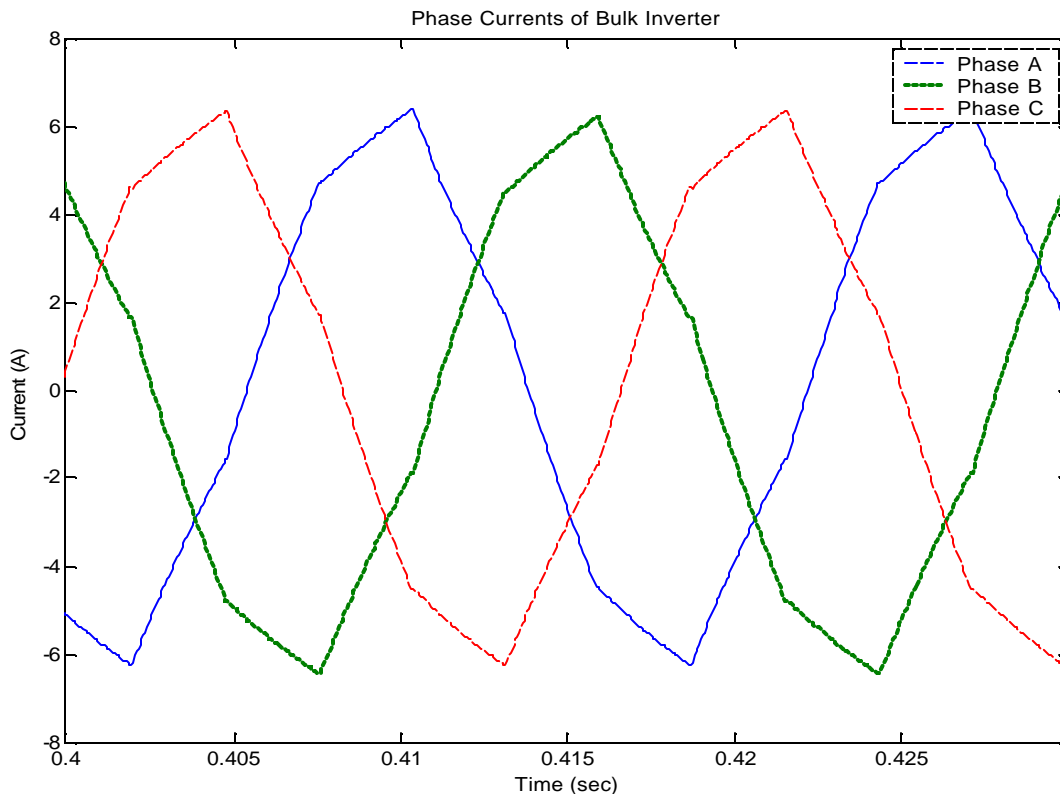


Figure 22. Phase A, B, and C currents of the bulk inverter ($DV_{dc} = 39 \text{ V}$).

The detailed view of the current waveforms reveals that the phase currents of the bulk inverter change in slope at six distinct points throughout the cycle. These points correspond to the switching events that occur every 2.8 ms, or 60° , to step the phase voltage to the a new level. Although the waveforms roughly follow the shape of the sinusoidal reference signal, the sharp corners at each transition point translate into higher frequency harmonics in the frequency spectrum of the waveform. The theoretical harmonic content of the current waveform can be derived from the magnitude of the harmonics present in the phase voltage waveform. The Fourier series expression for the six-step bulk inverter phase A voltage is [10]

$$v_{an} = \frac{2}{p} V_{dc} \cos q + \frac{2}{p} V_{dc} \sum_{k=1}^{\infty} \left(\frac{(-1)^{k+1}}{6k-1} \cos((6k-1)q) + \frac{(-1)^k}{6k+1} \cos((6k+1)q) \right) \quad (4-8)$$

The magnitude of the Fourier coefficients at each integer non-zero harmonic frequency for the bulk inverter current will follow the relation:

$$|I_n| = \left| \frac{B_n}{Z_n} \right|, \quad (4-9)$$

where I_n is the magnitude of n^{th} harmonic of phase current waveform, B_n is the magnitude of n^{th} harmonic of phase voltage, and Z_n is the load impedance at n^{th} harmonic frequency.

Since $n\omega_1 L > R$ for all harmonics, the impedance Z_n will be the dominant term in Equation 4-9. This will considerably decrease the magnitude of the higher harmonics of the load current waveform. Using the equations above, the frequency spectrum was predicted for the six-step bulk inverter operating with a dc bus voltage of 39 V. The results are depicted in Figure 23.

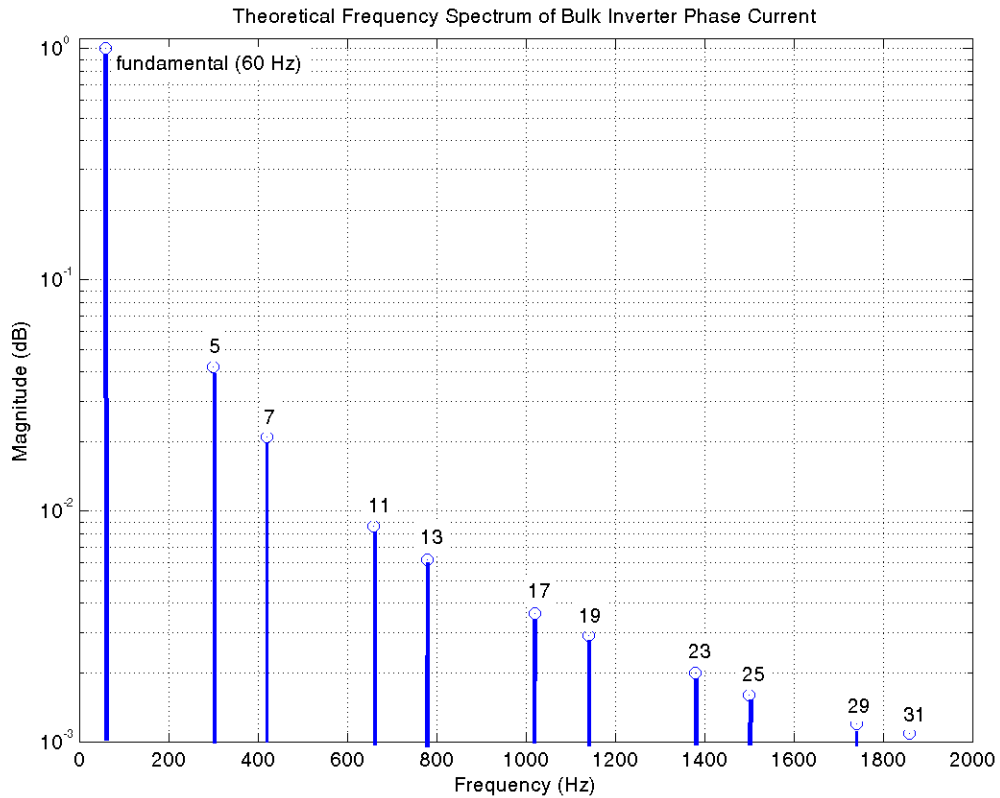


Figure 23. Theoretical harmonic content of bulk inverter phase current.

The number of each non-zero harmonic is depicted above each data point on Figure 23 where $Z_n = 1.05 + jn\omega_1 0.0091 \Omega$. The magnitude of each harmonic in the load current was computed in accordance with Equations 4-8 and 4-9. Using Equation 2-3, the theoretical THD of the six-step bulk inverter current was calculated to be 4.83% including the first 31 harmonics. Similar analysis revealed that the corresponding phase voltage waveform depicted in Figure 21 had a THD of 30.48%. This difference illustrates the significant effect that the load inductance has on the THD of the load current waveform.

This chapter presented the principles that govern the current produced by the hysteresis and bulk inverters. The expected current and voltage waveforms were created for the six-step bulk inverter using a MATLAB simulation. By apply-

ing the Fourier series expansion, the magnitude of the non-zero harmonics for the bulk inverter current waveform was computed. The theoretical THD of the phase current was 4.83% for the design load of 9.1 mH in series with a resistance of 1.05 Ω .

With the addition of the hysteresis inverter in parallel with the bulk inverter, the hybrid inverter system attempts to reduce this harmonic content. The next chapter will detail the results of the hardware implementation of the hybrid inverter system and measure its performance against the design goals.

THIS PAGE INTENTIONALLY LEFT BLANK

V. EXPERIMENTAL RESULTS

Following the completion of the hardware fabrication process, the hybrid inverter system was tested in several stages to assess its performance and determine the optimal operating mode. Each individual subsystem was tested before the system was configured to operate as a unit.

A. PRELIMINARY TESTING OF BULK INVERTER

The predicted performance characteristics of the six-step bulk inverter appear in the simulation results of the previous chapter. The simulation results served as a benchmark against which to measure the actual current waveform produced by the bulk inverter.

In the preliminary testing, the bulk inverter was connected to a floating-neutral, balanced, wye-connected load. Each phase of the load consisted of 9.1 mH inductance in series with 1.05 Ω of resistance. The resultant peak magnitude of the line-current was 5 A. The inductors used were the InverPower Controls reactor rated for 10 A continuous current and a total inductance of 42.5 mH and taps at 5% intervals. The load inductance of 9.1 mH was measured from the 30% tap of the inductor. The Hewlett-Packard 6002A DC Power Supply served as the dc-link voltage source with an overall range of 0–50 V for DV_{dc} . With $DV_{dc} = 39$ V, the bulk inverter produced the following current and voltage waveforms found in Figure 24 for each of the three phases.

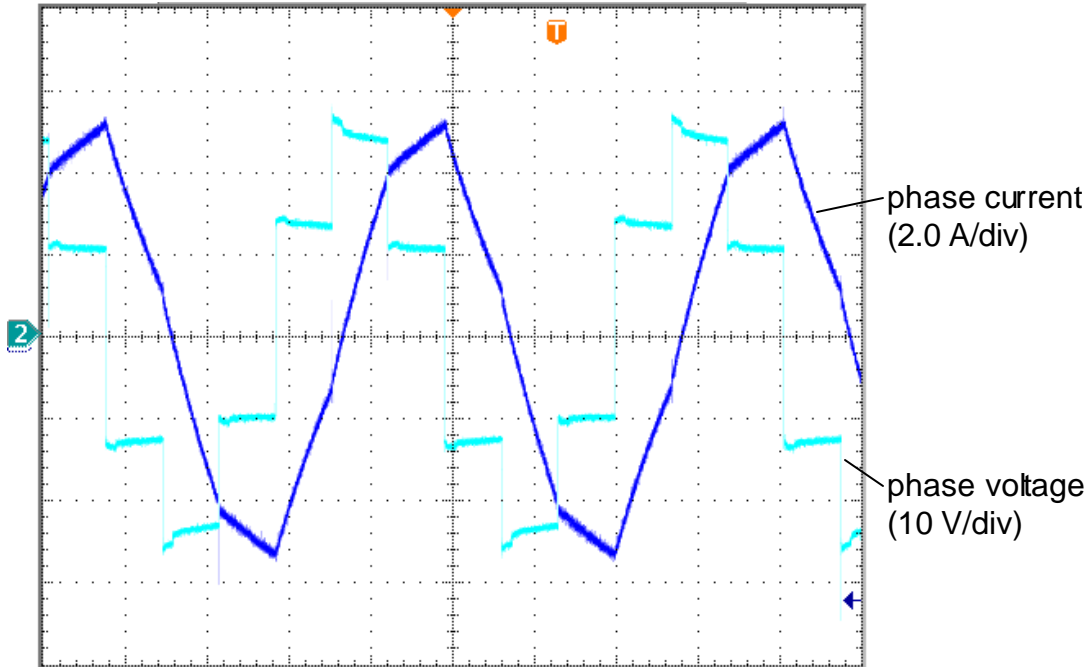


Figure 24. Bulk inverter phase current and voltage.

The bulk inverter voltage waveform in Figure 24 generally conformed to the six-step pattern of the simulation results depicted in Figure 21 in the previous chapter. Each change in the voltage level corresponded to a switching event, and voltage stepped through six discrete levels in the course of one cycle. The applied total voltage across the dc bus was 39 V for this test, as in the MATLAB simulation.

As the voltage steps through the sequence of levels, the phase current changes based on the RL load time constant and the applied voltage. The current changes at the fastest rate when the phase voltage reaches its minimum magnitude of 24 V as seen in Figure 24. Since the load is inductive, the current lags the voltage by 85° .

The experimental phase shift was greater than the phase shift of 75° observed in the MATLAB simulation. The difference was most likely caused by a discrepancy in the measured inductance and the actual inductance of the load L at 60 Hz. Since the actual inductance of inductors used in the experiment vary with frequency [2], the load may have actually had more inductance at 60 Hz

than the value measured by the instrument. This would cause the phase shift to be higher.

Although they both follow the same overall pattern, the results from the simulation did predict a higher peak value of the current (6.0 A) than the current produced by the actual hardware (5.4 A). The 10% error in the experimental current magnitude compared to the simulation results was most likely caused by the errors in the inductor values mentioned above, underestimated voltage drops in the IGBT switches and diodes, or switching delay times. Other than this difference, the actual results corresponded with the current waveforms produced in the simulation.

The six-step bulk inverter performed as predicted by the theoretical analysis and it proved suitable for coupling with the hysteresis inverter to form the hybrid inverter system.

B. THREE-PHASE TESTING OF HYSTERESIS INVERTER

The hysteresis inverter had been built and tested during a previous research effort with good results as an independent unit [2]. The original testing provided baseline results. The baseline results used a dc bus voltage of 20 V and a load of 9.1 mH in series with a 1- Ω resistance. A peak load current of 2 A was produced with a hysteresis band of 0.06 A. However, in order to use this inverter with the bulk inverter in the hybrid system, the three-phase reference signal must come from the bulk inverter and not the original hysteresis inverter signal generator. Therefore, independent testing of the hysteresis inverter was repeated using the hysteresis signal reference circuit (Figure 15) at the baseline and then at the desired 5-A system peak load current. The three-phase output current is depicted in Figure 25.

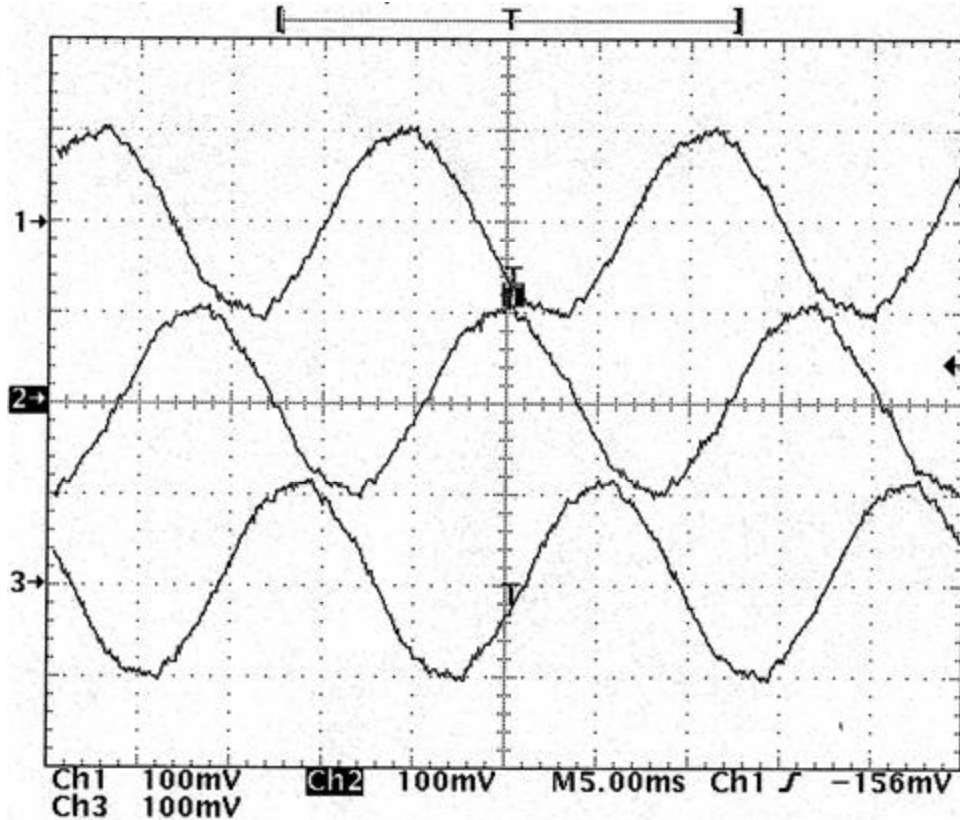


Figure 25. Phases A (top), B (middle), and C (bottom) of hysteresis inverter operating independently with $I_h = 0.1$ A and $DV_{dc} = 39$ V. (5.0 A/div)

The results depicted in Figure 25 confirm that the hysteresis inverter worked as designed with the new hysteresis signal reference circuit created for the hybrid inverter system. The testing done in the previous research effort was revalidated as the current waveform matched the sinusoidal reference signal at 5 A peak magnitude.

C. SINGLE-PHASE PARALLEL TESTING

Prior to commencing testing and optimization of the complete three-phase hybrid inverter system, a preliminary trial of one individual phase was conducted to verify that the bulk and hysteresis inverters would work in conjunction with one another. The results closely resembled the waveforms produced in Reference 2. The parallel combination of one phase of the bulk inverter and one phase of the hysteresis inverter produced a sinusoidal output current to a load of 9.1 mH in

series with a $1.05\text{-}\Omega$ resistance. Tests of the other two phases yielded similar results.

The single-phase experimental trials revalidated the previous results and confirmed that the parallel combination of the bulk and hysteresis inverter elements would work together as designed.

D. THREE-PHASE PARALLEL TESTING

After seeing acceptable results during single-phase testing, the hybrid inverter system was reconfigured for three-phase operation. The objective of the testing was to provide answers to the following questions:

- Can the hybrid inverter system produce a high-fidelity sinusoid from the reference?
- How can the hybrid inverter system be optimized to draw all of the fundamental load current from the bulk inverter and minimize the current produced by the hysteresis inverter?

Variables in the hybrid inverter system that could be controlled were the width of the hysteresis band, the phase shift between the bulk and hysteresis inverters, the input dc bus voltage level, the composition of the load, and the size of the load combining reactances. The experimental process aimed to adjust each of these independent parameters to find the optimal combination to produce the waveform that most closely matched the sinusoidal reference signal. In addition to obtaining the highest quality load current waveform, the secondary objective was to minimize the magnitude of the current produced by the hysteresis inverter at the fundamental frequency and to make the bulk inverter produce virtually all of the useful power. Minimizing the current share of the hysteresis inverter would enable the smallest possible hysteresis inverter to be used and it would make the overall hybrid inverter system more compact.

The hybrid inverter was configured as depicted in Figure 18 with each inverter phase output passing through a 9.1-mH inductor and then into the common phase load of a $1.05\text{-}\Omega$ resistor. The neutral point was floating in the middle of the balanced wye-connected load. After several iterative adjustments to the

dc bus voltage, the phase shift between inverters, and the width of the hysteresis band, the optimal operating point was found. The phase currents from phases A, B, and C at the optimal operating point are shown from top to bottom respectively in Figure 26.

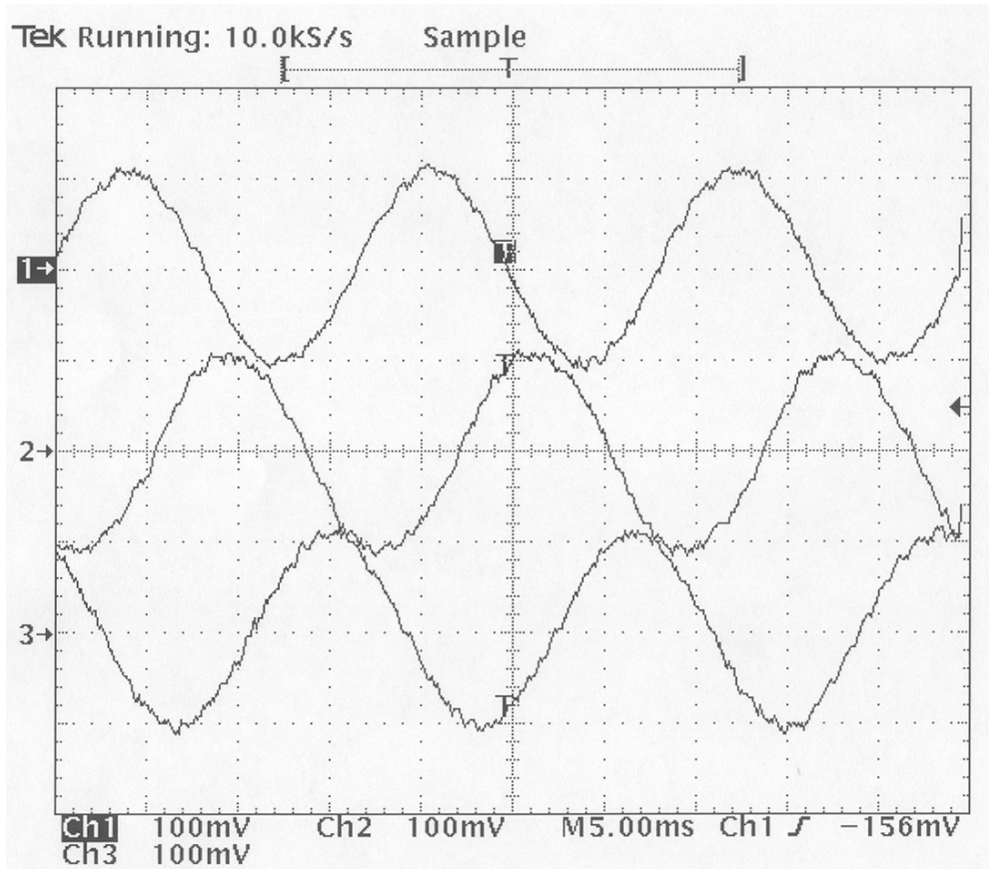


Figure 26. Phases A, B, and C in parallel operation (5.0 A/div).

In order to produce these results, the phase shift between the bulk and hysteresis inverters was 55° , the dc bus voltage ΔV_{dc} was set to 30.8 V, and the width of the hysteresis band I_h was approximately 0.1 A. Figure 27 shows a closer view of the three phase currents on the same x-axis.

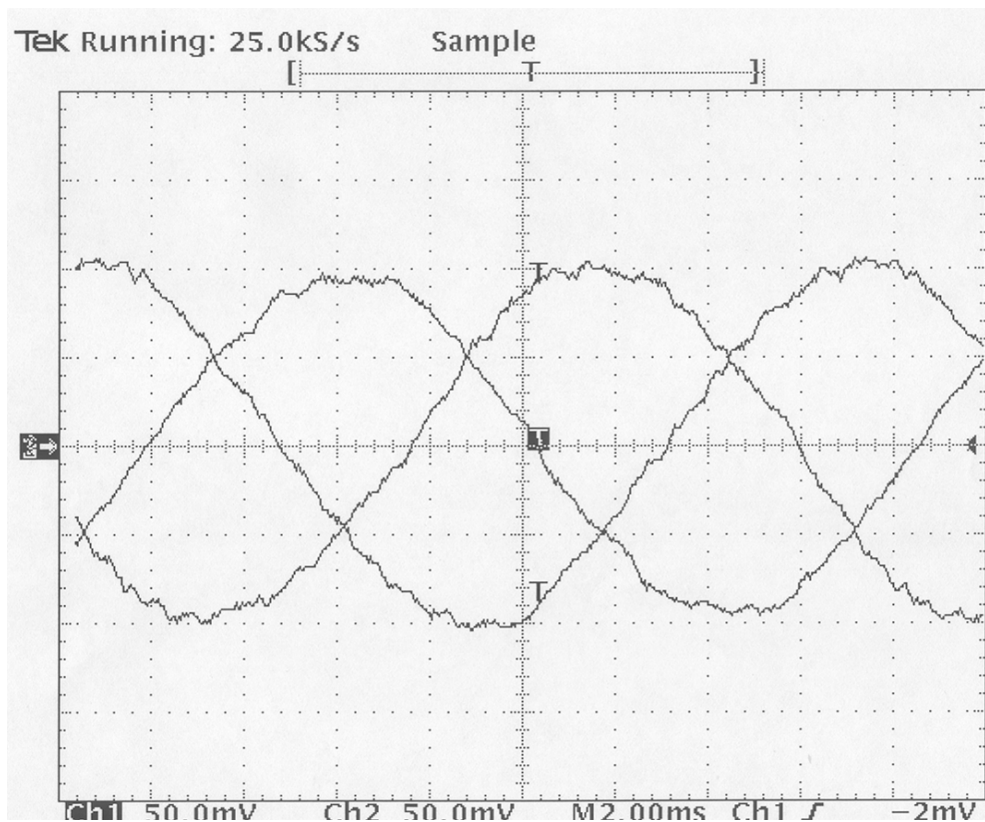


Figure 27. Detailed view of phase A, B, and C currents (2.5 A/div).

The above figures affirm that the output current of the hysteresis inverter coupled in parallel with the bulk inverter closely resembles a sinusoid.

The objective of the hybrid inverter was to produce a high-fidelity load current waveform and reduce the THD of the bulk inverter load current. The output current waveforms of both the hybrid inverter and the bulk inverter operating independently were analyzed using the Hewlett Packard 3561A Dynamic Signal Analyzer. The frequency spectrum of a representative phase of the load current produced by the bulk inverter appears below in Figure 28.

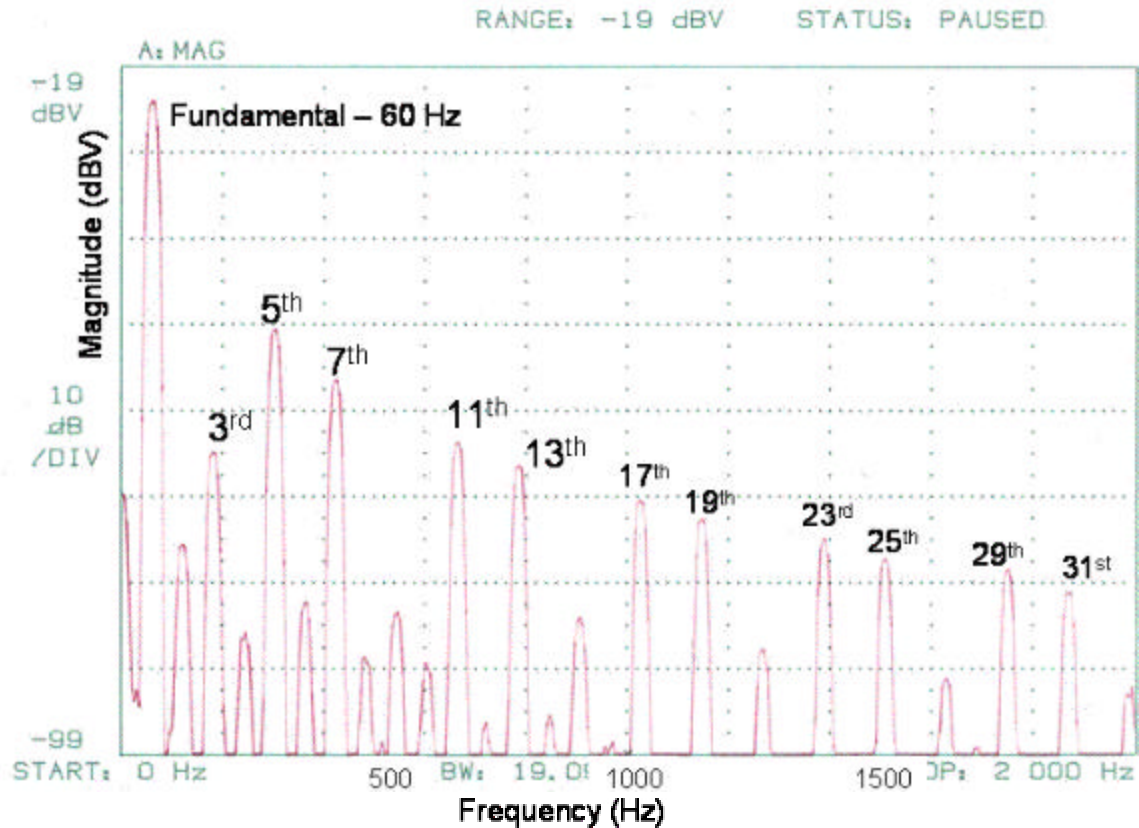


Figure 28. Frequency spectrum of bulk inverter (10 dB/div, 0-2000 Hz).

The observed frequency spectrum of the bulk inverter closely resembles the predicted harmonic content shown in Figure 23 in the previous chapter. Including the first 20 harmonics, the current THD was calculated to be 5.5% by the spectrum analyzer. This experimental THD was slightly higher than the theoretical THD of 4.83%. The actual THD was most likely higher because the odd triplet harmonics are suppressed but not completely cancelled as in the theoretical calculations.

Although the bulk inverter did produce a load current with relatively low harmonic content, the addition of the hysteresis inverter further reduced the overall THD. The frequency spectrum of the hybrid inverter phase load current is shown in Figure 29.

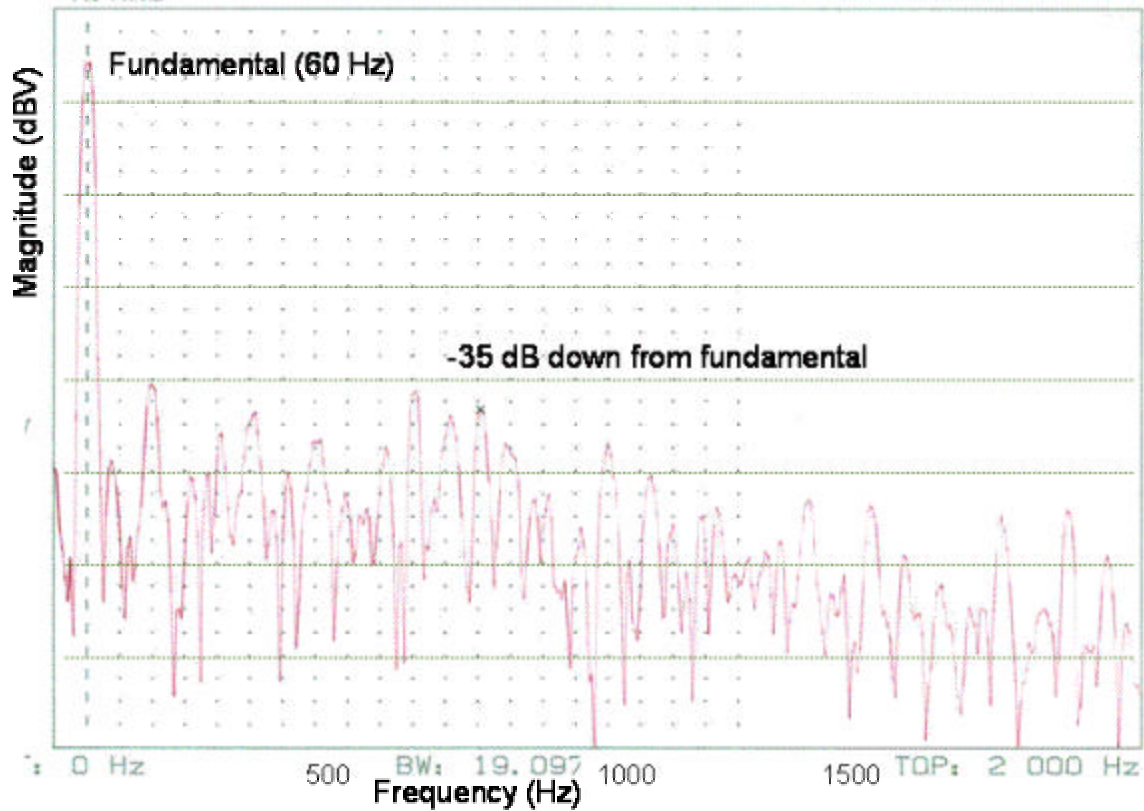


Figure 29. Frequency spectrum of hybrid inverter (10 dBV/div, 0-2000 Hz).

Figure 29 shows that the lower-order harmonics were at least 35 dB smaller than the fundamental for the hybrid inverter. The fifth and seventh harmonics made the largest contribution to the THD in the bulk inverter, but they were attenuated by at least 10 dB in the hybrid frequency spectrum. The percentage THD was 3.2% for the hybrid inverter spectrum up to the 20th harmonic. Since the hysteresis inverter switched at a variable frequency, the harmonics produced by the switching operations were spread across the spectrum and did not appear as a dominant harmonic at a fixed frequency.

Based on the frequency spectrum analysis, the addition of the hysteresis inverter improved the overall THD of the load current waveform of the bulk inverter from 5.5% to 3.2%. These results affirmed that the hybrid inverter could produce a high-fidelity output load current.

Although the hybrid inverter met its overall objective to produce a clean sinusoidal output current, it fell short of the design goal of limiting the fundamental current to the bulk inverter. While phase B of the hysteresis inverter produced only canceling harmonics, phases A and C provided a share of the fundamental load current.

In the phase A load current depicted in Figure 30, the bulk inverter provides approximately 3.5 A of the 5.0 A total current across the load while the hysteresis inverter makes up the difference with the other 1.5 A. Ideally, the bulk inverter would produce about 5.0 A at the fundamental frequency while the hysteresis inverter only injected current to cancel harmonics higher than 60 Hz in the bulk current waveform.

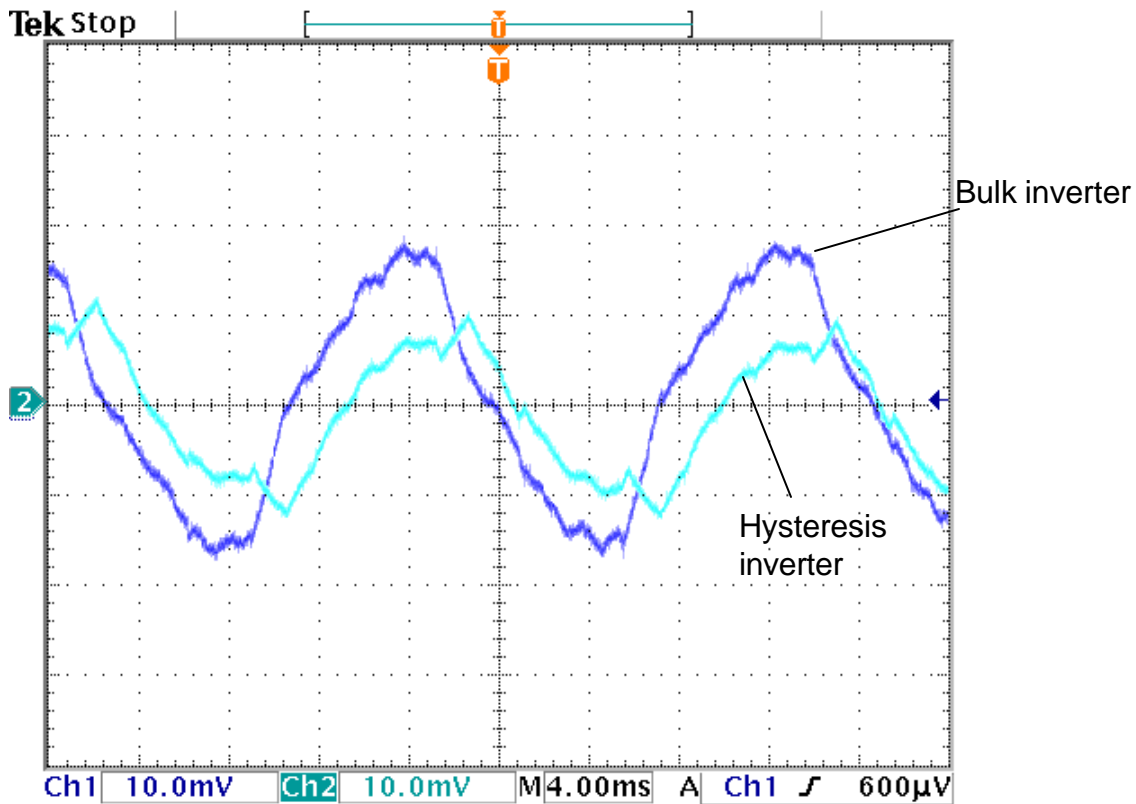


Figure 30. Hybrid Phase A – Bulk and Hysteresis phase currents (2A/div).

Figure 31 shows the results for phase B. The currents for each inverter element in phase B approach the ideal objective described above. It contributes

almost no current at the fundamental frequency of 60 Hz. The bulk inverter in phase B produced about 4.8 A peak at the fundamental frequency, while the hysteresis inverter current stayed below 1 A for the entire cycle. As expected, the hysteresis inverter switched at a frequency much higher than the fundamental in order to cancel the harmonics and to maintain the sinusoidal shape of the load current waveform.

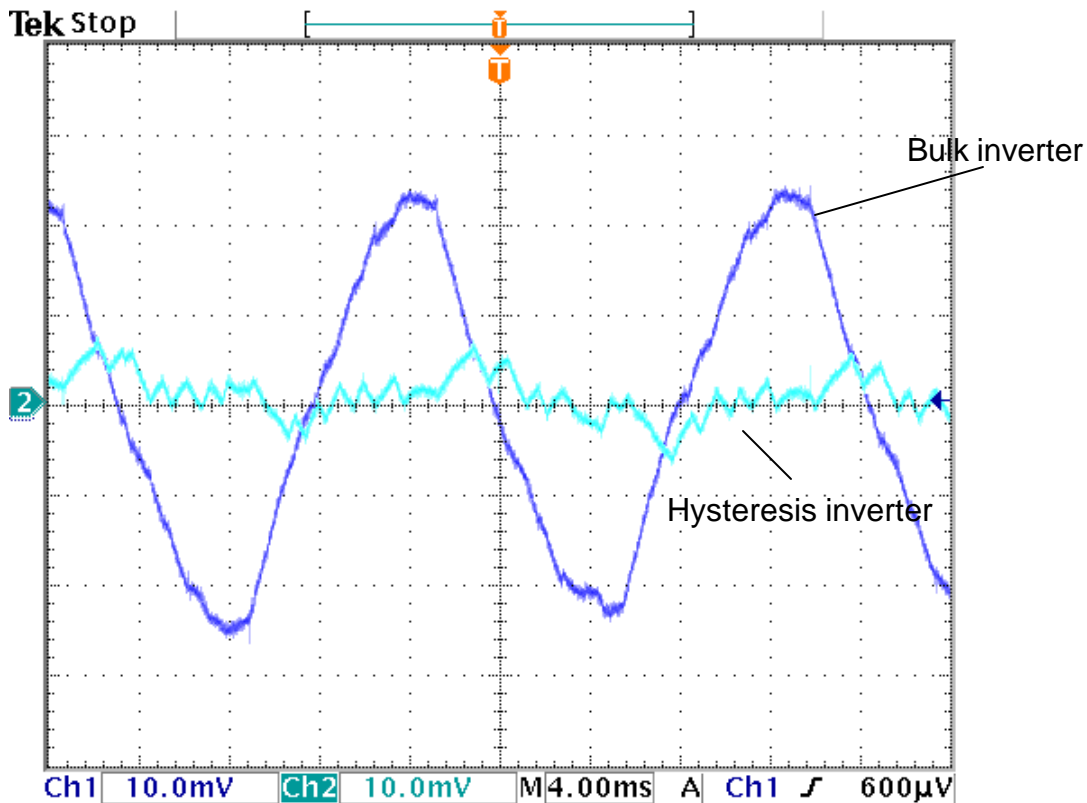


Figure 31. Hybrid Phase B – Bulk and Hysteresis phase currents (2 A/div).

The balance between the bulk and hysteresis inverter currents for phase C appears in Figure 32. As in phase A, phase C of the hysteresis inverter contributed a portion of the load current at the fundamental frequency. The results are slightly more optimal than those of phase A. Thus, the hysteresis inverter provides the right amount of current to augment the 4.0-A peak produced by the bulk inverter.

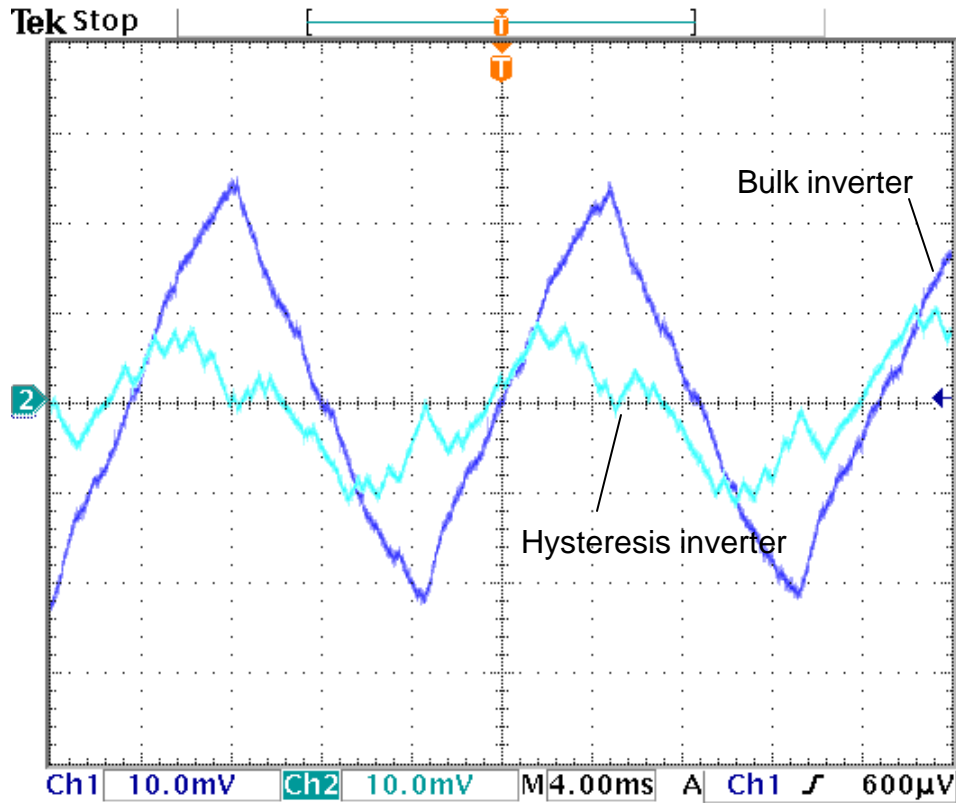


Figure 32. Hybrid Phase C – Bulk and Hysteresis phase currents (2 A/div).

E. ZERO-SEQUENCE CURRENT

In a balanced, three-phase system, the sum of the three phase currents will add to zero for any time in the cycle due to the 120° phase separation between each of the current vectors. The currents theoretically will comply with the following relation:

$$i_a(t) + i_b(t) + i_c(t) = 0. \tag{5-1}$$

The instantaneous sum of all three phase currents is called the zero-sequence current. The zero-sequence current should stay at zero at all times during the cycle.

However, the experimental testing of the three-phase hybrid inverter revealed a small but persistent zero-sequence current present in the circuit. Although it did not disrupt the three line current waveforms, the zero-sequence cur-

rent appeared as a low frequency oscillation on the input current waveforms from the hysteresis inverter and the bulk inverter. Connecting the two inverters in parallel created a path for the zero-sequence current to flow. Figure 33 depicts the effect of the zero-sequence current and the ripple caused by it on the output currents of the bulk and hysteresis inverters.

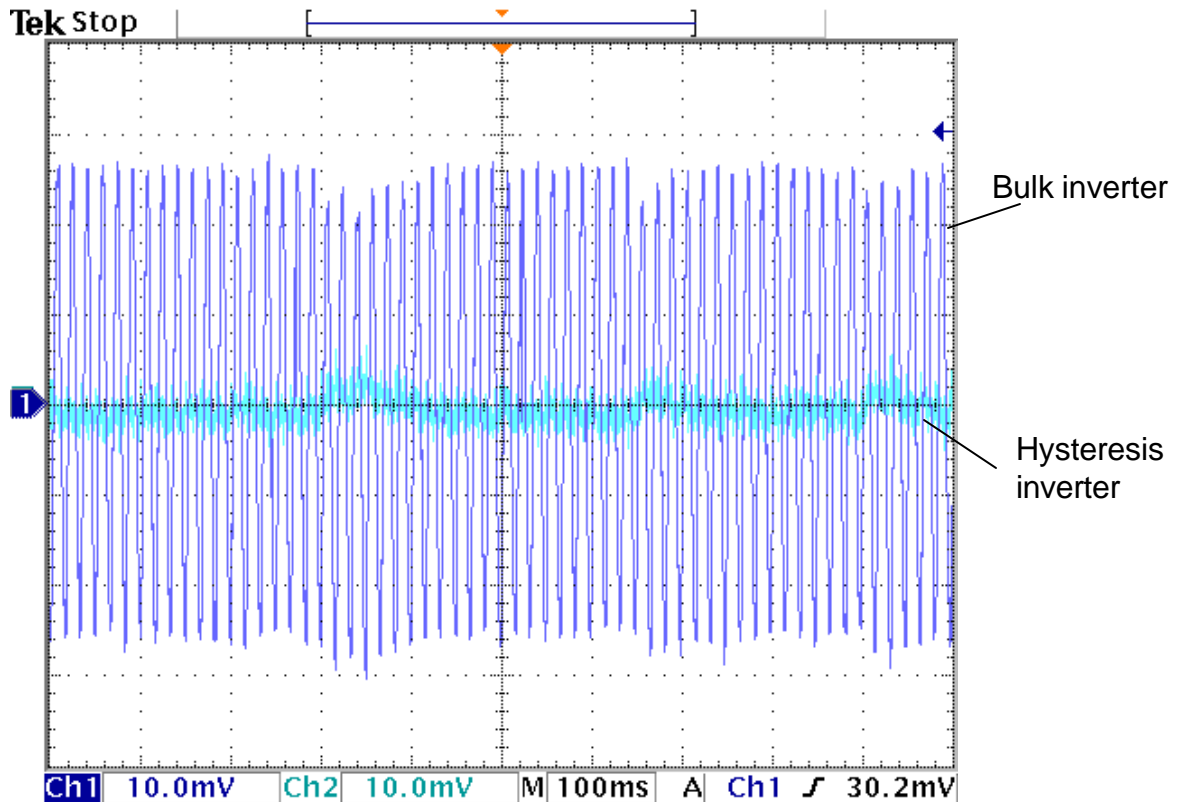


Figure 33. Effect of zero-sequence current on hybrid circuit (2 A/div)

The large amplitude waveform represents the bulk inverter current and the smaller amplitude waveform near the x-axis traces the hysteresis inverter current. The zero-sequence current causes the ripple in the two waveforms at low frequency over several cycles. This low frequency ripple caused the jitter in the waveforms when observed on the oscilloscope. Figure 33 shows the dynamic interaction between the inverters as the hysteresis inverter current increased when the bulk inverter decreased.

The zero-sequence could be caused by a slight imbalance in the actual phase shift between current vectors, a small difference in the load impedances,

or the dynamic interaction between the inductors connected to the hysteresis and bulk inverters on each phase.

In an attempt to eradicate the zero-sequence current, the neutral point was temporarily clamped to the midpoint of the dc bus. This modification had no effect on the oscillations caused by the zero-sequence current, so the neutral point was returned to its floating state. An unbalanced load was the suspected cause of the zero-sequence current. However, more precise matching of the load elements failed to correct the problem.

One effective way to eliminate the zero-sequence current as well as the imbalance between phase currents would be to implement a new control strategy in the quadrature-direct-zero (qd0) reference frame. Common in motor drive control, the qd0 strategy would provide control over the composite three-phase system by transforming the three phase currents into two equivalent orthogonal quantities and a zero-sequence term [10].

F. SUMMARY OF RESULTS

In the experimental testing phase of this research effort, the hybrid inverter system was evaluated against expected performance parameters to validate the design. After verification of each subsystem independently, the hysteresis inverter was coupled in parallel with the bulk inverter and tested in its design configuration to verify that it met the prescribed objectives.

The testing revealed that the hysteresis/bulk hybrid inverter produced a high-fidelity load current waveform with a peak amplitude of 5 A. The addition of the hysteresis inverter to the bulk inverter significantly reduced the THD of the current waveform. Therefore, the first objective of the testing was met as the hybrid inverter produced a high-fidelity sinusoid from the reference.

The second objective was to optimize the system such that all of the fundamental current was produced by the bulk inverter. Thus, the power output of the hysteresis inverter would be minimized. This load-sharing strategy would capitalize on the strengths of each inverter element and allow for smallest possible hysteresis inverter. Experimental results revealed that the optimal operating

point was achieved at a dc bus voltage of 30.8 V, a phase shift of 55° (between the bulk and hysteresis inverters), and a hysteresis band of 0.1 A. However, a larger than desired portion of the fundamental load current was contributed by the hysteresis inverter despite attempts to draw all of the fundamental load current from the bulk inverter. It became clear that a further refinement of the control strategy would be necessary to alleviate an imbalance caused by zero-sequence current.

THIS PAGE INTENTIONALLY LEFT BLANK

VI. CONCLUSION

With the experimental testing complete, the results can be measured against the original research questions. The results of this thesis effort also bring up new initiatives and further questions for future exploration.

A. REVIEW OF RESEARCH QUESTIONS AND GOALS

This research effort sought to explore the concept of a hybrid inverter consisting of a high fidelity hysteresis element coupled with a lower fidelity six-step inverter. The goal was to verify that the two types of inverters would operate together in a parallel connected configuration with a balanced three-phase load. The overall objective was to improve the fidelity of the bulk inverter output by adding the hysteresis inverter. Experimental testing strived to determine the optimal operating point for the system where the hysteresis inverter delivered only enough current to cancel the higher harmonics of the bulk inverter. The output current waveforms for each phase were evaluated and compared to the desired 60-Hz sinusoidal reference current signal.

B. SUMMARY OF EXPERIMENTAL RESULTS

After the construction and preliminary testing of the six-step bulk inverter, the hybrid inverter was configured by connecting the bulk inverter in parallel with the existing hysteresis inverter across a three-phase balanced load. The hybrid inverter produced a satisfactory three-phase output current at a level of 5.0 A peak for each phase in experimental trials. The THD of the current waveform improved from 5.5% for the bulk inverter alone to 3.2% for the hybrid combination of the bulk and hysteresis inverters. The bulk inverter produced almost all of the load current at the fundamental frequency in phase B, but the hysteresis inverter contributed some of the fundamental load current in phases A and C. There was also a small zero-sequence current present in the system which caused a low frequency oscillation in the individual output waveforms of the hysteresis and bulk inverters. The closed-loop feature of the hysteresis inverter enabled the hybrid inverter to maintain a stable output current despite these disturbances.

During the experiment, the independent inputs of dc bus voltage, phase shift between inverters, and hysteresis tolerance band were adjusted to determine the mode which produced the best results. Iterative trials revealed that a dc bus voltage of 30.8 V, a phase shift of 55°, and a hysteresis band of 0.1 A defines the optimal operating point for the system. The hybrid system produced a high-fidelity current waveform at a frequency of 60 Hz and a magnitude of 5.0 A.

C. ANSWERS TO RESEARCH QUESTIONS BASED ON RESULTS

The experimental results obtained in this research effort validate the concept of the hybrid inverter consisting of a hysteresis inverter and a six-step bulk inverter connected in parallel. The addition of the hysteresis inverter offered an overall improvement to the quality of the output of the bulk inverter and made a higher quality current waveform. The hysteresis inverter also closes the current control loop to respond to anomalies and disturbances in the system and ensure that the load receives a constant, sinusoidal current at the desired magnitude. The optimal operating point for the paralleled inverters was found after fine tuning the input variables.

Although trials were conducted at a relatively low power level, the hybrid system can be easily scaled to higher power levels with no modification. The hybrid inverter developed in this thesis represents a viable alternative to existing converter technology in providing a reliable current source for motor drives on today's naval vessels.

D. RECOMMENDATIONS FOR FURTHER DEVELOPMENT

This thesis represents only one phase in an ongoing effort to fully develop the hybrid inverter for employment in motor drive systems. While the questions presented in this research effort were answered, additional questions were created and more study is required to bring this concept into practical use.

As discussed in Chapter 5 previously, a zero sequence current caused a low frequency oscillation in the circuit. Also, the output phase currents of the hysteresis inverter did not all carry the same amount of current. This is not surprising, since all three phases are controlled independently. A new control

scheme implementing the $qd0$ reference frame could potentially remedy these issues and provide even more fidelity to the output waveform.

Since the hybrid inverter system was tested at a lower power level, further testing needs to be performed at high power levels to verify its capability. The actual bulk and hysteresis inverters were designed for much higher power in their present configuration. They are only limited by the ratings of the IGBTs in their respective power sections. It is estimated that the existing hybrid inverter system could produce up to 100 kW at 480 V given a sufficient source and load.

The hysteresis inverter currently in use implements a two-state switching algorithm to keep the current within the hysteresis band. It switches the phase voltage between $+V_{dc}$ and $-V_{dc}$ as the current goes below and above the hysteresis band. Although this mode of operation produces satisfactory results, the simulation performed in Reference 2 demonstrated that superior performance could be achieved by the implementation of three-state switching. This improved mode would switch the phase voltage between $+V_{dc}$ and 0 when the reference current is increasing and alternate the voltage applied between $-V_{dc}$ and 0 when the reference is decreasing. A modification or redesign of the existing hardware would be necessary to add this feature to the hybrid inverter, but it could potentially improve the fidelity of the output current.

THIS PAGE INTENTIONALLY LEFT BLANK

APPENDIX A. CIRCUIT WIRING DIAGRAMS

This appendix provides the specific layout and pin connections for the circuits described in Chapter 3.

Figure 34 displays the layout of the components on the main circuit board for the bulk inverter controller. The 60 Hz signal generator, the phase-shifter circuits, and the comparator circuits are on this board. Tables 2–14 list the specific pin connections for each 16-pin socket.

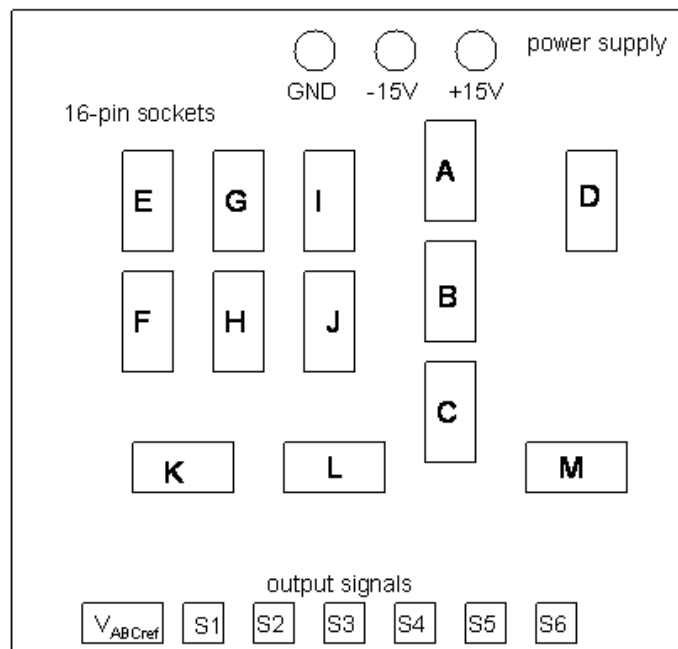


Figure 34. Component Layout Diagram for Bulk Inverter Controller.

Pin #	Tie to	component	Tie to	Pin #
1	V_{Aref}	LF347	NC	16
2	A9		NC	15
3	B10		NC	14
4	+15V		-15V	13
5	D2		D7	12
6	C10		D13	11
7	V_{Bref}		V_{Cref}	10
8	GND	10 k Ω	B1	9

Table 2. Socket A wiring diagram.

Pin #	Tie to	component	Tie to	Pin #
1	A9	20 k Ω	B15	16
2	A1	300 Ω	B16	15
3	B9	24 k Ω	B13	14
4	A1	1 k Ω	B14	13
5	A3	24 k Ω	B11	12
6	GND	1 k Ω	B12	11
7	GND	0.1 μ F	A3	10
8	A3	0.1 μ F	B3	9

Table 3. Socket B wiring diagram.

Pin #	Tie to	component	Tie to	Pin #
1	-15V	3 k Ω	C15	16
2	A1	1 k Ω	C16	15
3	A1	1 k Ω	C13	14
4	+15V	3 k Ω	C12	13
5	A2	- diode 1 +	C13	12
6	C16	- diode 2 +	A2	11
7	A1	100 k Ω	A6	10
8	A7	100 k Ω	C10	9

Table 4. Socket C wiring diagram.

Pin #	Tie to	component	Tie to	Pin #
1	C7	43 k Ω	D15	16
2	A5	3 k Ω	D16	15
3	D2	+ 0.1 μ F	GND	14
4	A7	100 k Ω	A11	13
5	A10	100 k Ω	D13	12
6	D4	43 k Ω	D10	11
7	A12	3 k Ω	D11	10
8	D7	+ 0.1 μ F	GND	9

Table 5. Socket D wiring diagram.

Pin #	Tie to	component	Tie to	Pin #
1	GND	0.1 μ F	+15V	16
2	GND	2 k Ω	E5	15
3	GND	LM311 comparator	E16	14
4	K16		Logic1	13
5	M1		NC	12
6	E9		NC	11
7	E13	510 Ω	E16	10
8	GND	0.1 μ F	-15V	9

Table 6. Socket E wiring diagram.

Pin #	Tie to	component	Tie to	Pin #
1	GND	0.1 μ F	+15V	16
2	GND	2 k Ω	E4	15
3	GND	LM311 comparator	E16	14
4	M2		Logic2	13
5	K15		NC	12
6	E9		NC	11
7	E13	510 Ω	E16	10
8	GND	0.1 μ F	-15V	9

Table 7. Socket F wiring diagram.

Pin #	Tie to	component	Tie to	Pin #
1	GND	0.1 μ F	+15V	16
2	GND	2 k Ω	G5	15
3	GND	LM311 comparator	G16	14
4	K12		Logic3	13
5	M1		NC	12
6	I9		NC	11
7	I13	510 Ω	G16	10
8	GND	0.1 μ F	-15V	9

Table 8. Socket G wiring diagram.

Pin #	Tie to	component	Tie to	Pin #
1	GND	0.1 μ F	+15V	16
2	GND	2 k Ω	H4	15
3	GND	LM311 comparator	H16	14
4	M2		Logic4	13
5	K11		NC	12
6	H9		NC	11
7	H13	510 Ω	H16	10
8	GND	0.1 μ F	-15V	9

Table 9. Socket H wiring diagram.

Pin #	Tie to	component	Tie to	Pin #
1	GND	0.1 μ F	+15V	16
2	GND	2 k Ω	I5	15
3	GND	LM311 comparator	I16	14
4	I16		Logic5	13
5	M1		NC	12
6	E9		NC	11
7	E13	510 Ω	I16	10
8	GND	0.1 μ F	-15V	9

Table 10. Socket I wiring diagram.

Pin #	Tie to	component	Tie to	Pin #
1	GND	0.1 μ F	+15V	16
2	GND	2 k Ω	J4	15
3	GND	LM311 comparator	J16	14
4	M2		Logic6	13
5	I15		NC	12
6	J9		NC	11
7	J13	510 Ω	J16	10
8	GND	0.1 μ F	-15V	9

Table 11. Socket J wiring diagram.

Pin #	Tie to	component	Tie to	Pin #
1	V _{Aref} (A1)	1 k Ω	E4	16
2	K1	1 k Ω	F5	15
3	E4	100 k Ω	E13	14
4	F4	100 k Ω	F13	13
5	V _{Bref} (A7)	1 k Ω	G4	12
6	K6	1 k Ω	H5	11
7	G4	100 k Ω	G13	10
8	H4	100 k Ω	H13	9

Table 12. Socket K wiring diagram.

Pin #	Tie to	component	Tie to	Pin #
1	V _{Cref} (A10)	1 k Ω	I4	16
2	L1	1 k Ω	J5	15
3	I4	100 k Ω	I13	14
4	J4	100 k Ω	J13	13
5				12
6				11
7				10
8				9

Table 13. Socket L wiring diagram.

Pin #	Tie to	component	Tie to	Pin #
1	E4/G4/I4	10 k Ω	E16	16
2	E5/G5/J5	10 k Ω	E9	15
3				14
4				13
5				12
6				11
7				10
8				9

Table 14. Socket M wiring diagram.

The components of the hysteresis signal reference circuit are contained on a separate board. Figure 35 illustrates the layout of the hysteresis signal reference circuit.

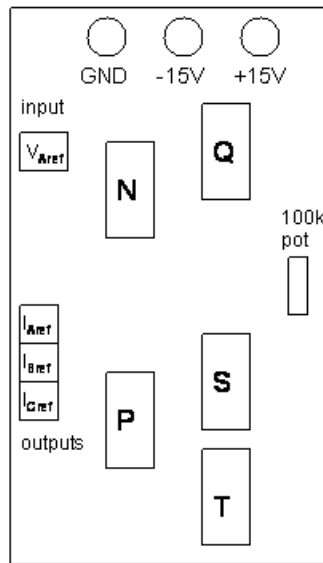


Figure 35. Component Layout Diagram for Hysteresis Signal Reference Circuit.

The specific pin connections for the hysteresis signal reference circuit appear in Tables 15–20.

Pin #	Tie to	component	Tie to	Pin #
1	Q15	LF347	R2	16
2	Q16		R16	15
3	Q3		R3	14
4	N9		Q9	13
5	Q6		P2	12
6	Q4		Q10	11
7	Q12		Q8	10
8	GND	0.1 μ F	+15V	9

Table 15. Socket N wiring diagram.

Pin #	Tie to	component	Tie to	Pin #
1	S11	LF347	NC	16
2	S5		NC	15
3	T4		NC	14
4	N9		Q9	13
5	T1		T2	12
6	S14		S10	11
7	I _{Aref}		S8	10
8	P3	0.1 μ F	GND	9

Table 16. Socket P wiring diagram.

Pin #	Tie to	component	Tie to	Pin #
1	V _{Aref}	20 k Ω	N2	16
2	Q16	10 k Ω (R _f)	N1	15
3	N3	10 k Ω	GND	14
4	N6	10 k Ω	Q15	13
5	Q4	10 k Ω	S3	12
6	N5	5 k Ω	GND	11
7				10
8	GND	0.1 μ F	-15V	9

Table 17. Socket Q wiring diagram.

Pin #	Tie to	component	Tie to	Pin #
1				16
2				15
3	pot1/Q12	100 k Ω	P6	14
4	P5, I _{Aref}	100 k Ω	S14	13
5	P2	100 k Ω	S4/T3	12
6	S5	100 k Ω	I _{Bref}	11
7	P1	100 k Ω	P11	10
8	P10, I _{Cref}	100 k Ω	S10	9

Table 18. Socket S wiring diagram.

Pin #	Tie to	component	Tie to	Pin #
1	P5/pot2	0.1 μ F	GND	16
2	P12	0.1 μ F	GND	15
3	S12	43 k Ω	T13	14
4	P3	3 k Ω	T14	13
5	S7	43 k Ω	T11	12
6	T2	3 k Ω	T12	11
7				10
8				9

Table 19. Socket T wiring diagram.

Pin #	Tie to	component	Tie to	Pin #
1	P5	100 k Ω pot	T1	2

Table 20. Potentiometer (R_i) connections.

THIS PAGE INTENTIONALLY LEFT BLANK

APPENDIX B. MATLAB SIMULATION CODE

The following MATLAB script file was written to simulate the performance of the six-step bulk inverter.

Filename: sixstepinverter.m

```
% Terence White
% simulation of six-step bulk inverter current and voltage
clear
simlength=3.5; % length of simulation in seconds
N=30000; % number of data points
t=linspace(0,simlength,N); % time vector
dt=simlength/N; % time increment for simulation
L=9.1e-3; % load parameters
R=1.05; % for each phase
w=377; % frequency in rad/s
xl=w*L; % reactance of load
Z=sqrt(xl^2+R^2); % impedance magnitude
tau=R/L; % RL time constant of load
Vsw=4; % forward voltage drop of two switches (typical=2V per IGBT)
k=1;
ia0=0;
ib0=0;
ic0=0;
t0=0;
ia=zeros(1,N);
ib=zeros(1,N);
ic=zeros(1,N);
Va=zeros(1,N);
Vb=zeros(1,N);
Vc=zeros(1,N);
E=39; % applied dc bus voltage in volts
step=1;
tprime=dt;
theta=1;
for k=1:N
    theta=tprime*w;
    if theta>=0 & theta<=pi/3 % first voltage step
        step(k)=1;
        Va(k)=(E-Vsw)/3;
        Vb(k)=-2*(E-Vsw)/3;
        Vc(k)=(E-Vsw)/3;
        tprime=tprime+dt;
```

```

end
if theta>pi/3 & theta<=2*pi/3 % second voltage step
    step(k)=2;
    Va(k)=2*(E-Vsw)/3;
    Vb(k)=-(E-Vsw)/3;
    Vc(k)=-(E-Vsw)/3;
    tprime=tprime+dt;
end
if theta>2*pi/3 & theta<=pi % third voltage step
    step(k)=3;
    Va(k)=(E-Vsw)/3;
    Vb(k)=(E-Vsw)/3;
    Vc(k)=-2*(E-Vsw)/3;
    tprime=tprime+dt;
end
if theta>pi & theta<=4*pi/3 % fourth voltage step
    step(k)=4;
    Va(k)=-(E-Vsw)/3;
    Vb(k)=2*(E-Vsw)/3;
    Vc(k)=-(E-Vsw)/3;
    tprime=tprime+dt;
end
if theta>4*pi/3 & theta<=5*pi/3 % fifth voltage step
    step(k)=5;
    Va(k)=-2*(E-Vsw)/3;
    Vb(k)=(E-Vsw)/3;
    Vc(k)=(E-Vsw)/3;
    tprime=tprime+dt;
end
if theta>5*pi/3 & theta<=2*pi % sixth voltage step
    step(k)=6;
    Va(k)=-(E-Vsw)/3;
    Vb(k)=-(E-Vsw)/3;
    Vc(k)=2*(E-Vsw)/3;
    tprime=tprime+dt;
end
if theta>2*pi % resets algorithm to first step
    tprime=0;
    theta=0;
    step(k)=1;
end
if k>1
if step(k)>step(k-1) % reset current initial conditions
    ia0=ia(k-1); % after each step starts
    ib0=ib(k-1);
    ic0=ic(k-1);

```

```

        t0=tprime;
    end
    if step(k)<step(k-1)
        ia0=ia(k-1);
        ib0=ib(k-1);
        ic0=ic(k-1);
        t0=tprime;
    end
    % generate the load current vectors
    ia(k)=exp(-tau.*(tprime-t0)).*ia0+(Va(k-1)./R).*(1-exp(-tau.*(tprime-
t0)));
    ib(k)=exp(-tau.*(tprime-t0)).*ib0+(Vb(k-1)./R).*(1-exp(-tau.*(tprime-
t0)));
    ic(k)=exp(-tau.*(tprime-t0)).*ic0+(Vc(k-1)./R).*(1-exp(-tau.*(tprime-
t0)));
    end
    % generate line-to-line voltage
    vab(k)=Va(k)-Vb(k);
    k=k+1; % advance to next increment
end
figure(1)
plot(t,Va,t,ia)
AXIS([0.4 0.5 -25 25])
figure(2)
plot(t,ibref,t,ib)
AXIS([0.4 0.5 -6 6])
figure(3)
plot(t,ia,t,ib,t,ic)
AXIS([0.4 0.5 -6 6])

```

THIS PAGE INTENTIONALLY LEFT BLANK

LIST OF REFERENCES

- [1] "Advanced Electrical Power Systems Thrust," Office of Naval Research website, www.onr.navy.mil, last accessed 30 May 2004.
- [2] Paul Fillmore, "Design, construction, and testing of a hysteresis controlled dc-ac power converter for paralleling," Master's thesis, Naval Postgraduate School, Monterey, California, 2003.
- [3] Ned Mohan, Tore M. Undeland, and William P. Robbins, *Power Electronics*, 3rd Edition, pp. 40-42, 204-239, John Wiley and Sons, Inc., Hoboken, New Jersey, 2003.
- [4] Shoji Fukuda and Masayuki Kitano, "Control strategy for a three-phase series-connected hybrid inverter system," *Proc. 2001 IEEE 32nd Annual Power Electronics Specialists Conference*, Vol. 2, pp. 968-973, IEEE Press, New York, 2001.
- [5] Andrzej M. Trzynadlowski, Niculina Patriciu, Frede Blaabjerg, and John K. Pedersen, "A hybrid, current-source/voltage-source power inverter circuit," *IEEE Transactions on Power Electronics*, Vol. 16, No. 6, pp. 866-871, 2001
- [6] Adel S. Sedra and Kenneth C. Smith, *Microelectronic Circuits*, 4th Edition, pp. 980-982, Oxford University Press, New York, 1998.
- [7] Robert F. Coughlin and Frederick F. Driscoll, *Operational Amplifiers and Linear Integrated Circuits*, 5th Edition, pp. 139-140, Prentice Hall, Upper Saddle River, New Jersey, 1998.
- [8] Robert Crowe, "Design, construction, and testing of a reduced-scale cascaded multi-level converter," Master's thesis, Naval Postgraduate School, Monterey, California, 2003.
- [9] Toshiba America Electronic Components, Inc., "IGBT New Products Guide," pp. 134-135, 1995.

[10] Paul C. Krause, Oleg Wasynczuk, and Scott D. Sudhoff, *Analysis of Electric Machinery and Drive Systems*, 2nd Edition, pp. 481-494, IEEE Press, New York, 2002.

INITIAL DISTRIBUTION LIST

1. Defense Technical Information Center
Ft. Belvoir, Virginia
2. Dudley Knox Library
Naval Postgraduate School
Monterey, California
3. Marine Corps Representative
Naval Postgraduate School
Monterey, California
4. Director, Training and Education, MCCDC, Code C46
Quantico, Virginia
5. Director, Marine Corps Research Center, MCCDC, Code C40RC
Quantico, Virginia
6. Marine Corps Tactical Systems Support Activity (Attn: Operations Officer)
Camp Pendleton, California
7. Dr. Robert Ashton, Department of Electrical and Computer Engineering
Code EC/Ah
Naval Postgraduate School
Monterey, California
8. Dr. Xiaoping Yun, Department of Electrical and Computer Engineering
Code EC/Yx
Naval Postgraduate School
Monterey, California
9. Dr. John Powers, Chairman, Department of Electrical and Computer
Engineering
Code EC
Naval Postgraduate School
Monterey, California
10. Major Terence H. White
Stafford, Virginia